Review

Spontaneous Directional Transportation Surface of Water Droplet and Gas Bubble: A Review

Yi Lu [1,†], Defeng Yan [1,†], Junyi Lin [1,†], Song Zhang [1] and Jinlong Song [1,2,*]

1 State Key Laboratory of High-Performance Precision Manufacturing, Dalian University of Technology, Dalian 116024, China; louis_13626240358@163.com (Y.L.); yandefeng1994@163.com (D.Y.); linjy1372@163.com (J.L.); zzhang_song1@163.com (S.Z.)
2 Key Laboratory for Micro/Nano Technology and System of Liaoning Province, Dalian University of Technology, Dalian 116024, China
* Correspondence: songjinlong@dlut.edu.cn
† These authors contributed equally to this work.

Abstract: The spontaneous directional transportation (SDT) of water and gas has functions such as efficient water collection, enhanced heat transfer, underwater drag reduction, and so on, having great application prospects in aerospace and navigation fields. Therefore, it is important to efficiently prepare spontaneous directional water droplet transportation (SDWT) surfaces and spontaneous directional gas bubble transportation (SDBT) surfaces and apply them in different fields. In recent years, researchers have used biological structures as the basis for their studies and have continued to analyze the SDT transport mechanism in depth, aiming to find more efficient transportation methods. In this review, we first summarize the important basic theories related to fluid transportation. Then, the related methods and the limitations corresponding to SDWT and SDBT are introduced and discussed. In addition, we review the applications of SDWT and SDBT. Finally, we highlight the challenges and future perspectives of SDWT and SDBT.

Keywords: spontaneous directional transportation; wettability gradient; shape gradient; cooperative surface

1. Introduction

In recent years, fluid transportation has gradually gained attention because of the development of precision medicine, micro-devices, and green energy collection. Researchers found that surfaces for water and gas transportation had numerous applications such as fog collection, heat transfer, drug transportation, and so on [1–7]. However, when a water droplet touches a solid surface, it will perform some indeterminate behaviors, such as impacting, jumping, trapping, and spreading. An underwater gas bubble demonstrates similar behaviors (adhesion, merging, etc.) when it contacts a solid surface. Researchers have undertaken many studies to make spontaneous directional transportation (SDT) possible, meaning that fluid can be transported on an expected trail.

Currently, the means of controlling fluid for spontaneous and directional transportation can be divided into two methods: fluid transportation using external energy and spontaneous directional fluid transportation without external energy input. Directional transportation using external energy is often achieved by magnetic field [8–10], electric field [11–13], thermodynamics [14,15], optics [16–18], and so on. Despite the fact that these methods can achieve directional fluid transportation, their application areas are limited due to the need for external energy input. Researchers have found that the spontaneous directional transportation of fluids without external energy input can also be achieved by using gravity or buoyancy. However, these methods can only transport fluid vertically upwards or downwards, and the accuracy of the fluid transportation is difficult to guarantee. When researchers studied organisms in nature, they found that many organisms had

evolved unique microstructures on their surfaces that enabled spontaneous directional water transportation (SDWT) and spontaneous directional gas bubble transportation (SDBT). Inspired by organisms in nature, researchers developed a variety of functional surfaces to enable spontaneous directional fluid transportation. The entire transportation process of the water droplet or gas bubble on functional surfaces does not require external energy input. Therefore, the application field of spontaneous directional fluid transportation will be more diversified in the future and is one of the key areas for the future development of fluid transportation systems. In 2001, Parker [19] from Oxford University found that numerous hydrophobic bulges and hydrophilic groove structures on the back of the desert beetle allowed the captured water droplet to be transported from its back to its mouth. The Janus membrane is also referenced, which is used for oil–water separation [20]. In 2012, Ju et al. [21] from Beihang University found that cacti evolved cone-shaped spines to adapt to desert environments. The fog droplets would spontaneously transport from the tip to the root due to the unbalanced Laplace pressure. Based on this, researchers designed a variety of structures inspired by the cactus spine for fog collection [22–24] and underwater gas supply [25]. In 2016, Chen et al. [26] found that water could transport continually on the peristome of nepenthes against gravity because of its multiscale structure, which optimized and enhanced the capillary force. Inspired by this, researchers designed an artificial bionic multiscale surface, which could control the water droplet transportation in a lab-on-a-chip device [27] and capture the bubbles underwater [28].

In this review, we first look back at the important basic theories related to fluid transportation. Then, we summarize the theories and methods of SDWT and SDBT and discuss their limitations. In addition, we review the applications of SDWT and SDBT in the fields of fog collection, fluid control, heat transfer, gas collection, and underwater sensors. Finally, we provide an outlook on the future of SDT based on the existing water droplet and gas bubble transportation methods and applications.

2. Basic Theories

The relevant basic theories of fluid transportation include contact angle, contact angle hysteresis, advancing contact angle, receding contact angle, sliding angle, three classical wettability models, surface tension, surface energy, and Laplace pressure. It is important to understand these theories to figure out the principle of SDT.

2.1. Contact Angle, Contact Angle Hysteresis, Advancing Contact Angle, Receding Contact Angle, and Rolling Angle

Contact angle θ is often used to characterize solid wettability. It is the angle between the tangent line of the gas–liquid interface and the solid–liquid line at the junction of gas, liquid, and solid phases. According to the different contact angles of water on the solid surface, the wettability of solid surface can be divided into four types: superhydrophilic ($0° \leq \theta \leq 10°$), hydrophilic ($10° \leq \theta \leq 90°$), hydrophobic ($90° \leq \theta \leq 150°$), and superhydrophobic ($150° \leq \theta \leq 180°$) [29–31]. In the case of the wettability of underwater gas bubbles on the solid surface, the wetting interface changes from a solid–liquid interface in air to a gas–solid interface in water, but the above theory is still valid.

For example, in the case of liquid, when delivering liquid to a droplet on a smooth and ideal solid surface, the contact line will move outward and keep the contact angle of the droplet the same. However, because the actual solid surface is rough and inhomogeneous, the contact line may not move with the increase in liquid volume. This phenomenon is called contact angle hysteresis. When delivering liquid to a droplet on a rough surface, the contact angle will increase because of contact angle hysteresis, and the contact angle at this time is named advancing contact angle θ_{ad}. The contact angle when the solid–liquid contact line is about to move forward is the maximum advancing contact angle, as shown in Figure 1a. On the contrary, removing liquid from a droplet on a rough surface causes the contact angle, called receding contact angle θ_{re}, to decrease. The contact angle when the solid–liquid contact line is about to move backward is the minimum receding contact

angle, as shown in Figure 1b. The contact angle hysteresis usually causes the drag force in SDWT, and the force F can be calculated by the following equation [32]:

$$F = \pi w \gamma (\cos \theta_{\mathrm{re}} - \cos \theta_{\mathrm{ad}}) \tag{1}$$

where w is the diameter of the solid–liquid contact surface and γ is the surface tension. On a tilted plane, the advancing angle and the receding angle of the liquid can also be observed. Due to the existence of the contact angle hysteresis, when the plane begins to tilt, the droplet does not immediately move. When the plane rotates to a certain angle, the droplet begins to roll. This angle is called rolling angle α. The degree of contact angle hysteresis determines whether the droplet is easy to roll.
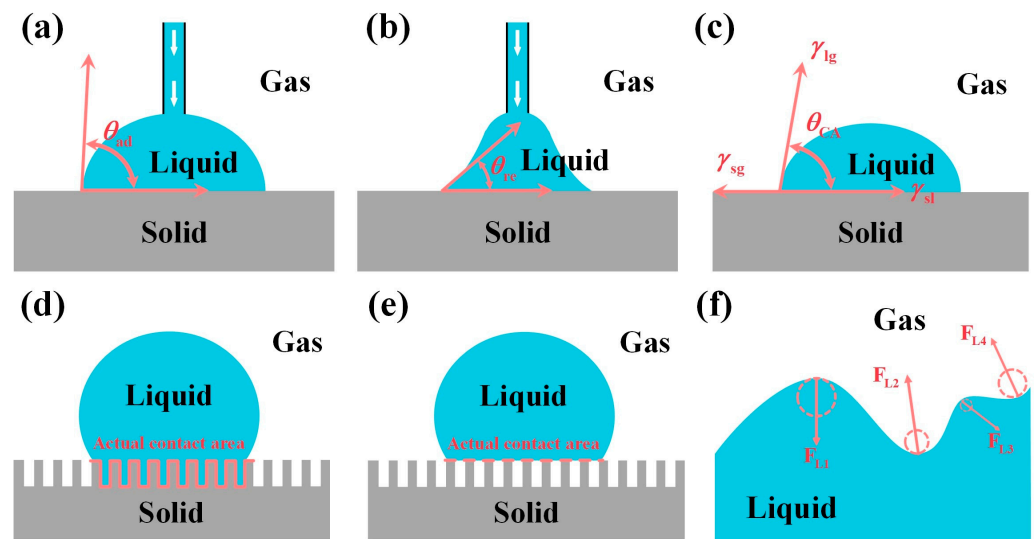

Figure 1. Wetting behavior of a droplet on a solid surface. (**a**) Advancing angle. (**b**) Receding angle. (**c**) Young model. (**d**) Wenzel model. (**e**) Cassie-Baxter model. (**f**) Laplace pressure.

2.2. Three Classical Wettability Models

The wetting behavior of a droplet on a solid surface can be summarized as follows: the Young model [33], the Wenzel model [34], and the Cassie–Baxter model [35], as shown in Figure 1c–e.

1. Young Model

The Young model is a model of a droplet on an ideal and smooth solid surface. It was proposed by Thomas Young in 1805, showing the connection between the surface tension and the static contact angle on an ideal smooth solid surface. The model equation is as follows:

$$\cos \theta_{\mathrm{e}} = \frac{\gamma_{\mathrm{SG}} - \gamma_{\mathrm{SL}}}{\gamma_{\mathrm{LG}}} \tag{2}$$

where θ_{e} is the eigen contact angle of the droplet to the solid; γ_{SG}, γ_{SL}, γ_{LG} are the surface tensions of the solid–gas interface, solid–liquid interface, liquid–gas interface.

2. Wenzel Model

Since the actual surface is not an ideal smooth surface, American researcher Robert N. Wenzel proposed the Wenzel model in 1936 based on the Young model. This model added the roughness factor, as follows:

$$\cos \theta_{\mathrm{a}} = r \frac{(\gamma_{\mathrm{SG}} - \gamma_{\mathrm{SL}})}{\gamma_{\mathrm{LG}}} = r \cos \theta_{\mathrm{e}} \tag{3}$$

where θ_a is the apparent contact angle, and r is the roughness factor which is equal to the ratio of the actual and the projection area of the rough surface. From the Wenzel model, it can be seen that the rougher surface will make the originally hydrophilic surface become more hydrophilic, and the originally hydrophobic surface will become more hydrophobic. The Wenzel model also explains that the surface of rose petals presents a superhydrophobic state but has a high adhesive force with water droplets. Jiang et al. studied and analyzed the phenomenon of the "petal effect" in 2008, and pointed out that the microstructure scale distribution of rose petal surface is the main factor affecting the adhesion of rose petals to water droplets [36,37]. The model successfully promotes the Young model to realistic situations but still fails to explain the low adhesion of water droplets on lotus leaves.

3.　Cassie–Baxter Model

To solve the limitation of the Wenzel model, Cassie and Baxter improved it in 1944. The Wenzel model pointed out that a droplet on a rough surface does not fill all the rough structures of a surface and leaves air in them. Based on this theory, they proposed the Cassie–Baxter equation:

$$\cos\theta_a = f_1 \cos\theta_e + f_2 \cos\theta_v \tag{4}$$

where f_1 and f_2 represent the liquid–solid contact area ratio and the liquid–air contact area ratio; θ_v is the eigen contact angle of the droplet to the gas. When it is a water droplet, since the eigen contact angle between water and air is 180°, the equation can be simplified as follows:

$$\cos\theta_a = f_1 \cos\theta_e - f_2 \tag{5}$$

From the above equation, it can be seen that when the eigen contact angle of the solid surface is a constant value, the contact angle will increase by decreasing the contact area. Since the water droplet in this model does not completely fill the rough structures of the surface, this helps the rolling of the water droplet. The reason why the droplets on lotus leaves show a superhydrophobic state and can roll off very easily can be explained using the Cassie–Baxter model. Ren et al. [38] prepared a biomimetic microarray surface by using shape memory polyurethane (SMP) as a substrate. With the help of SMP, the modulation of the surface morphology can be realized, and the droplets can be changed between the Wenzel and Cassie–Baxter models to achieve the difference in surface adhesion.

2.3. Surface Tension, Surface Energy, and Laplace Pressure

Surface tension is generated from the asymmetric force on the molecules of the surface. The direction of surface tension is the same as the tangent direction of the fluid surface layer. Surface energy is the energy required to extend a unit area of a material under constant temperature and pressure. Surface tension and surface energy of solid and liquid are key factors affecting surface wettability. For a liquid, surface tension and surface energy are numerically equal. Because of the energy minimization principle, the number of molecules in the surface layer of the liquid needs to be minimized, which causes the droplet to change its shape or position spontaneously. As shown in Figure 1f, for a liquid with a free interface, the force generated by the curve surface is named Laplace pressure. Its direction points to the center of the circle of the curvature, and the amount of force can be calculated by the following equation:

$$\Delta P = \frac{2\gamma}{R} \tag{6}$$

where R is the radius of curvature. Laplace pressure is an important driving force for SDWT. Thus, we can generate unbalanced Laplace pressure by changing the contact shape of the droplet to realize SDWT. The principle of SDBT using shape gradient characteristics same as SDWT.

3. Spontaneous Directional Transportation of Water Droplet (SDWT): Methods and Applications

In nature, plants and animals have evolved function surfaces due to their self-survival needs. By investigating these surfaces, researchers explored many function surfaces with gradient characteristics that can be used for efficient SDWT. An unbalanced Laplace force will be generated when a water droplet is on these surfaces, leading to SDWT. By reasonable design of the gradient characteristics of these surfaces, SDWT can be achieved. The gradient characteristics of these surfaces can be divided into three types: wettability gradient, shape gradient, and cooperative gradient.

3.1. SDWT Based on Wettability Gradient

The wettability gradient characteristic is the continuous change in the wettability on the surface. Since there are certain differences in the contact angle, advancing contact angle, and receding contact angle of the droplet on the surface with a wettability gradient, it will result in the spontaneous directional transportation of water droplets from the side that is not easily wetted to the side that is easily wetted.

In 1978, Greenspan [39] first predicted that a water droplet could directionally transport on a surface with the wettability gradient through theoretical and analytical modeling derivations. In 1992, Chaudhury et al. [40] prepared a surface with wettability gradients by exposing a polished silicon wafer to the diffusing front of a vapor of decyl trichlorosilane. On this surface, water droplets showed a contact angle ranging from 25° to 97°. For the first time, water droplets could transport against gravity on a 15° tilted plane with a speed of 1 mm/s to 2 mm/s. In 2001, this team also similarly created a sample that had a contact angle of 100° in the surface center and a contact angle of 0° at the surface edge [41]. They performed condensation tests on this surface; as shown in Figure 2a, droplet 1 and droplet 3 spontaneously transported through the sample surface within 0.033 s, and droplet 2 did not move significantly at first due to its location. However, at 0.466 s, the position of droplet 2 had changed, which caused droplet 2 to be quickly transported across the surface within the next 0.033 s. Feng et al. [42] developed a method by controlling the distance between the electrodes to achieve differences in chemical composition on the surface, as shown in Figure 2b. Water droplets could spread spontaneously up to 4 mm and transport against gravity on this surface. This method can quickly create a surface with a wettability gradient on different conductive metals. In 1997, Wang et al. [43] produced TiO_2-coated glasses with a wettability gradient using UV irradiation, which enabled the use of light to control the chemical composition. After that, Ito et al. [44] developed a photodegradation technique to fabricate a wettability gradient by controlling the light intensity and duration. As shown in Figure 2c, a 2 μL water droplet can transport on this surface at a maximum speed of 6 mm/s and a maximum distance of 3.5 mm. Hong et al. [45] changed the oxidizer concentration by diluting it and controlled the oxidation time to oxidize vinyl-terminated self-assembled monolayers (SAMs) to carboxylic acid (COOH)-terminated SAMs. The behavior of droplet transportation on this surface is shown in Figure 2d. This is a simple preparation process and allows the generation of gradients at multiple points on the surface. Hernández [46] also produced a chemical composition gradient on the graphene surface using plasma processing in conjunction with a mask, which has the advantages of convenience, flexibility, controllable process, and environmental friendliness (Figure 2e).
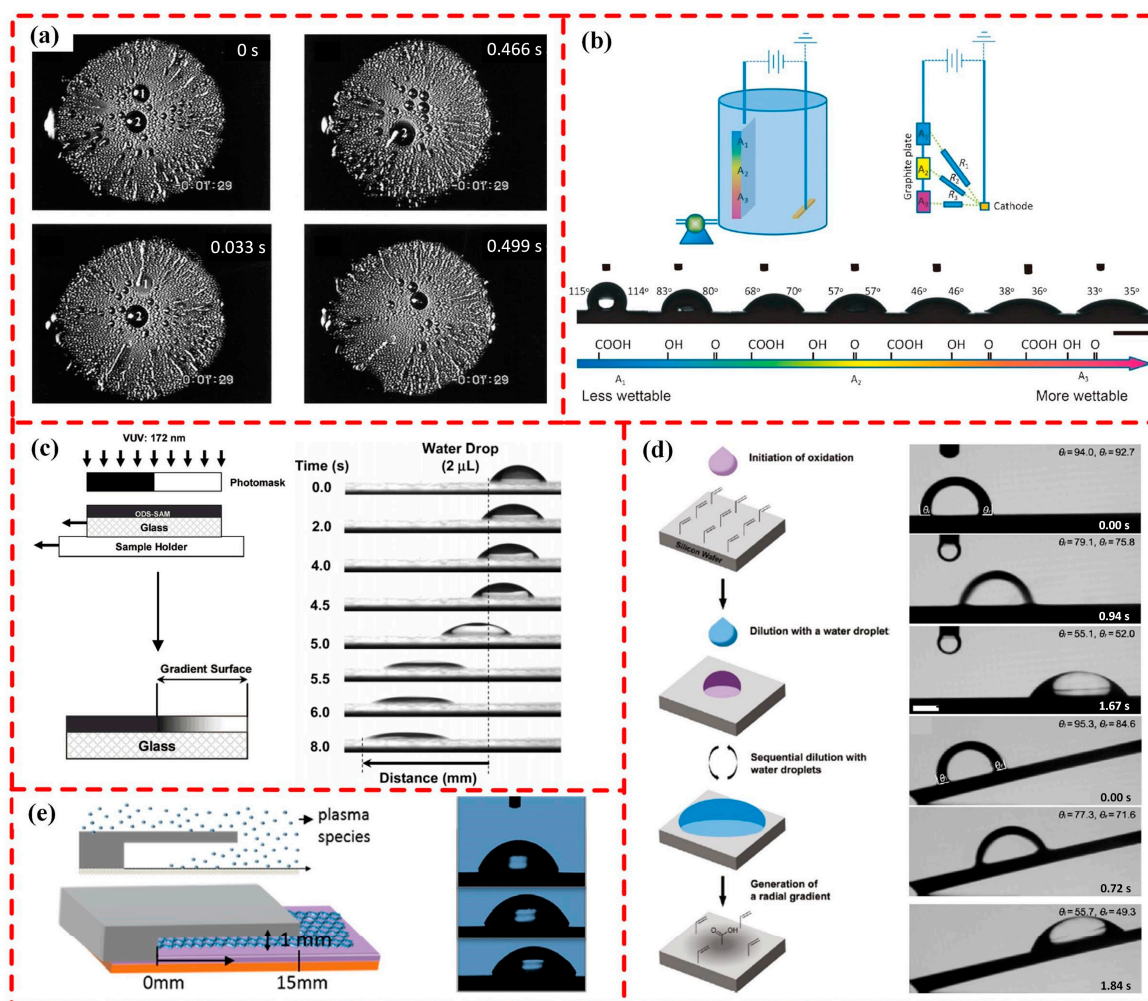
Figure 2. Fabrication and droplet motion behavior on the surface with wettability gradient caused by different surface compositions. (**a**) Condensation and droplet transportation on surface fabricated by vapor phase diffusion. Reproduced with permission from [41], Copyright 2001, *Science*. (**b**) Schematic illustration of the formation of wettability gradients on a graphite plate and water contact angles along the gradient surface. Reproduced with permission from [42], Copyright 2014, *Angew. Chem. Int. Ed.* (**c**) Droplet motion behavior on wettability gradient surfaces fabricated by photolithography. Reproduced with permission from [44], Copyright 2007, *Langmuir*. (**d**) Fabrication and droplet motion behavior on the surface generated by controlled surface reactions. Reproduced with permission from [45], Copyright 2010, *Langmuir*. (**e**) A well-controlled chemical gradient on the surface fabricated by plasma processing. Reproduced with permission from [46], Copyright 2013, *ACS Nano*.

According to the Wenzel model, it can be seen that the contact angle of the surface with lower surface roughness is also smaller. Thus, a water droplet will spontaneously and directionally transport from the hydrophilic area with higher roughness to that with lower roughness. He et al. [47] bonded a thin polydimethylsiloxane (PDMS) membrane on the top of a rough PDMS substrate and deflected it pneumatically, which achieved a wettability gradient using roughness difference for the first time. This method did not change the chemical composition of the surface and developed a new strategy for the fabrication of wettability gradients. Zhu et al. [48] fabricated square columns with different side lengths, heights, and spacing on the silicon surface by photolithography, which caused the roughness difference. Inspired by this, Sun et al. [49] proposed a surface with different roughness by changing the laser processing parameters. On this surface, the contact angle of the water droplet ranges from 126° to 145° and the surface can achieve SDWT (Figure 3a).

Chu et al. [50] fabricated nano-pillars using photolithography and plasma etching, and then tilted these nanopillars by the stresses generated by unilateral gold film on nano-pillars. Its surface nanostructure and water droplet transportation are shown in Figure 3b. Li et al. [51] created a V-shaped array on the surface of an elastic material. By changing the curvature of the elastic film, the parameters of the V-shaped arrays can also be changed, which might lead to a difference in the wettability gradient. When the curvature changes, the water can be transported in different directions. In addition to the above methods, O. Bliznyuk [52] presented a way to change the ratio of hydrophilic and hydrophobic regions of a surface to achieve a wetting gradient. The schematic illustration of the structure and the droplet motion behavior are shown in Figure 3c. Similarly, Liu et al. [53] fabricated a wettability gradient (CA = 15.5°~166°) by etching silicon nanopillars and adjusting the area of hydrophilic silica planes. As shown in Figure 3d, the speed of the droplet can be up to 75 mm/s, and the droplet can transport in curves along a designed track. In addition, Huang et al. [54] used photolithography combined with low surface energy modification to fabricate circular arrays with different diameters and spacings on the copper surface. On this surface, a water droplet could easily transport past the surface within 2.5 s.
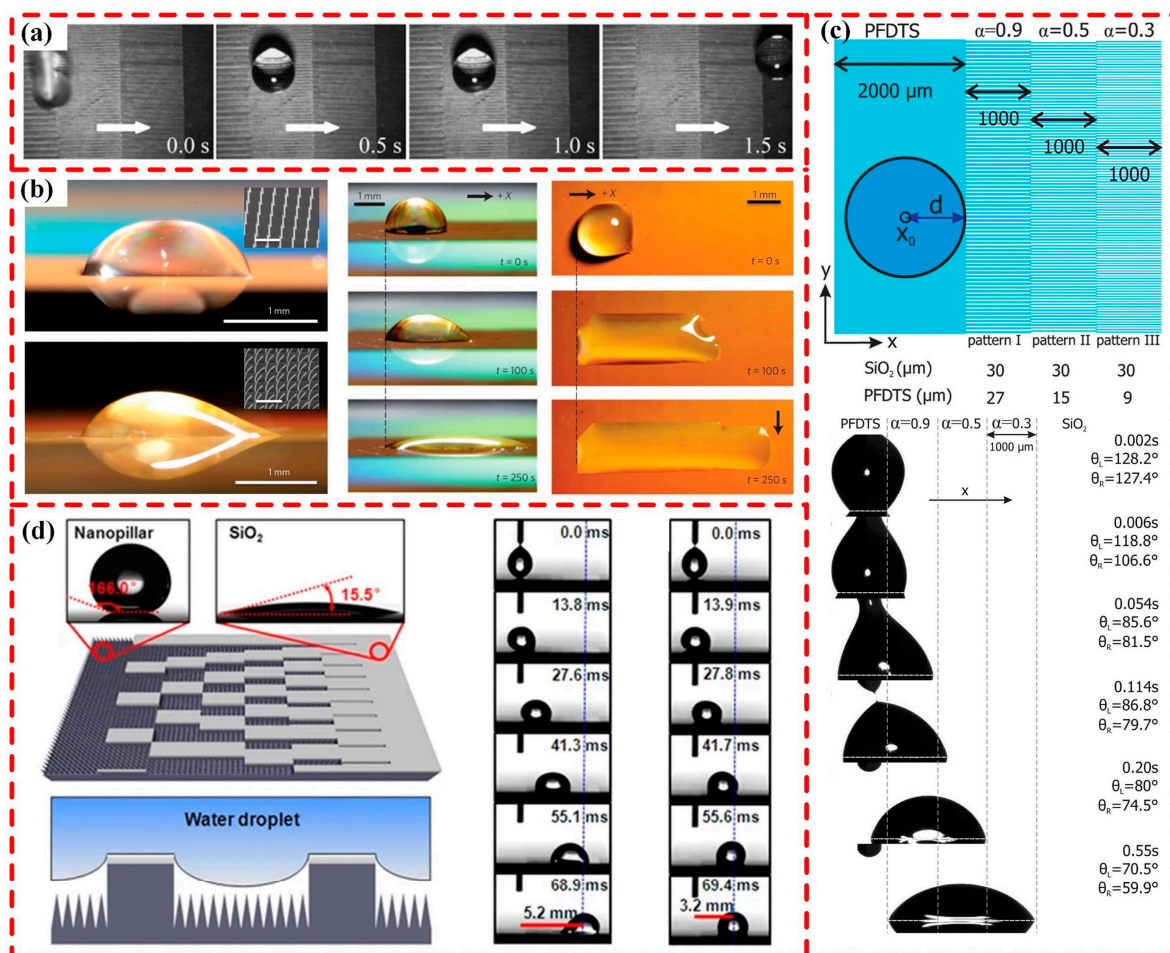

Figure 3. Wettability gradient caused by different surface roughness. (**a**) Water transportation on a laser-etched surface. Reproduced with permission from [49], Copyright 2008, *Thin Solid Films*. (**b**) Nanostructure and water droplet motion behavior of surfaces with different nanopillars. Reproduced with permission from [50], Copyright 2010, *Nature Materials*. (**c**) Structure of a surface that has different ratios of hydrophilic and hydrophobic regions and water droplet motion behavior on it. Reproduced with permission from [52], Copyright 2011, *Langmuir*. (**d**) Wetting behavior and water droplet motion behavior of a surface consisting of hydrophobic silica nanopillars and hydrophilic SiO$_2$. Reproduced with permission from [53], Copyright 2017, *Scientific Reports*.

The surface with a wettability gradient for water droplet transportation was one of the first areas that researchers began to study. Many researchers focused on the fabrication of wettability gradient surfaces using more convenient processing methods. However, the commonly used processing methods, such as vapor phase diffusion [39–41,55], SAMs remold [44,45], photolithography [43,48,50,54], and so on, are still complex and unsuitable for large-area processing. But most wettability gradient surfaces have hydrophilic regions that leave water stains after droplet transportation. This will change the former wettability gradient, resulting in unsustainable transportation.

3.2. SDWT Based on Shape Gradient

Shape gradient means that there is no change in the wettability of the sample surface, and the water droplet transportation is only caused by the macro/micro morphology of the surface. When a water droplet falls on a surface with a shape gradient, it will be driven by the Laplace force, resulting in SDWT. Shape gradient characteristics can usually be divided into two types: using a cone-like shape to make the droplet subjected to unsymmetrical Laplace pressure and using a repetitive array structure to make the droplet subjected to the unbalanced force, causing them to diffuse directionally.

3.2.1. Cone-like Shape

Cone shapes formed between non-parallel plates are the most common three-dimensional asymmetric structures. The shape gradient characteristics caused by cones can be divided into concave curvature gradients on the inner surface of the cone (Figure 4a) and convex curvature gradients on the outer surface (Figure 4b). The concave curvature gradient on the inner surface of the cone causes the water droplets inside the cone to have an asymmetrically curved surface. This may result in the water droplets being affected by the unbalanced Laplace pressure and thus spontaneously transporting from a position of bigger curvature to a position of smaller curvature. In 1712, Hauksbee [56] first discovered that when oil of orange is placed between two glasses that are not parallel to each other, it will spontaneously transport towards the direction where the gap thickness is small. Prakash et al. [57] also discovered a way of SDWT inside a cone by studying the movement of the shorebird's beak during feeding, as shown in Figure 4c. The team designed a tweezer that can be controlled, and from theory, they analyzed SWDT between asymmetric plates that are repeatedly opened and closed [57,58].

Convex curvature gradients on the outer surface of the cone similarly result in an unbalanced Laplace pressure, driving the droplets at the outer surface of the cone from positions of smaller curvature to positions of larger curvature. In 1986, Carroll [59] discussed the balance of a water droplet on an elongated cylinder. McHale [60,61] calculated the surface energy of the water droplet by finite element analysis, explaining why small droplets on an elongated cylinder looked like a clamshell, while large droplets tended to form a barrel shape. Inspired by the above studies, Lorenceau et al. [62] showed a strategy for SDWT on a conical wire for the first time and pointed out the driving force was the Laplace pressure difference. Researchers focused on SDWT on a conical outer surface for a long time. They found that the conical structure of the cactus thorn helps it to easily collect water in deserts [21]. Xue et al. [63] found that the shape of the green bristlegrass bristle was a cone, with microgrooves on the surface, and had barbs so that the water droplets could spontaneously transport from the top of the bristle to the bottom (Figure 4d). Chen et al. [64] also pointed out that the water droplet on the setae of desert scorpions can achieve a fast speed. They found that the shape of the scorpion setae was also a cone, and it can accelerate the speed of water droplets to 100 mm/s by the water film caused by fog collection. Cone-like shapes can also be found on spider silk [65] and many other bionic, artificial fog-collecting surfaces [21,23,66,67].

Inspired by the cone-like shape of cactus thorns, the researchers proposed a wedge-shaped pattern on a flat surface. However, initially, the researchers did not realize that the wedge pattern could lead to SDWT, and they only created uniformly shaped tracks

on the super-wetted surface to control the route of the water droplet [68–70]. Until 2013, Alheshibri et al. [71] produced a wedge-shaped pattern by depositing hydrophobic copper on hydrophilic aluminum. When 2–80 μL of water droplets fell on the narrow side, they were able to transport from the narrow side of the wedge to the wide side of the wedge angle. They pointed out that the droplet motion behavior and the velocity of the water droplets depend on the wedge angle and the contact angle of the droplets on aluminum and copper. This study provides ideas and a basis for the SDWT on patterned super-wetted surfaces. As shown in Figure 4e, SDWT on a single wedge-shaped pattern (SWP) was noticed first. Ghosh et al. [72] used UV light in combination with a photomask to produce SWP and analyzed the motion behavior and force of the droplet on the pattern. The maximum water transportation flow rate of this pattern can reach 350 μL/s, and the maximum instantaneous speed of water droplets can reach 400 mm/s. This pattern also enabled droplet merging and anti-gravity transportation. In order to improve the transportation performance of SDWT, Liu et al. [73] fabricated SWP on a superhydrophobic aluminum by laser processing and studied the effect on transportation caused by different parameters of the laser processing. They pointed out that the microgrooves fabricated by laser processing led to faster water transportation speeds. SWP has shown excellent transportation performance in the field of SDWT. But because of its single wedge shape, it has a generous size at the end of the pattern, which may cause fluid loss. If the water droplet becomes smaller during transportation, the driving force coming from Laplace pressure will also be smaller, which results in a short transportation distance. To solve this problem, Liu et al. [74] proposed a superhydrophilic serial wedge-shaped pattern (SSWP) in which the wedges are connected head to tail (Figure 4f) to decrease fluid loss and increase the water transportation distance. However, this brings another problem: when the water droplets are at the junction of the pattern, they will be impeded by pinning force, which leads to a loss of speed. To solve the problem, researchers began to study the optimization of the junction. Liu et al. [74] proposed a method of arc junction transition optimization which increased the speed by 5 percent. Inspired by nepenthes, as shown in Figure 4g, Xie et al. [75] proposed a method of wedge junction transition optimization, resulting in the normalized transportation distance (transportation distance/droplet diameter) of 23.4 for a 3 μL droplet. Liu et al. [76] proposed a method of streamlined junction transition optimization, which allows large water droplets to pass the junction smoothly. However, a faster speed is always needed because of the significant use of SDWT. Yan et al. [77] were inspired by nepenthes and proposed a superhydrophilic serial cycloid-shaped pattern (SSCP). They replaced the wedge-shaped pattern with the cycloid-shaped pattern, which made the wedge angle continuously change during the transportation process and reduced the number of junctions (Figure 4h). The average water transportation speed within 50 mm on SSCP was 40% higher than that of the SSWP.

These methods all have a cone-like shape and use the different Laplace pressures caused by the shape to achieve SDWT (from narrow to wide). This water transportation type has potential applications in fog collection, microfluidic devices, microchemical reactors, and liquid mixing [78,79]. But it has the disadvantages of fixed transportation routes and fluid loss.
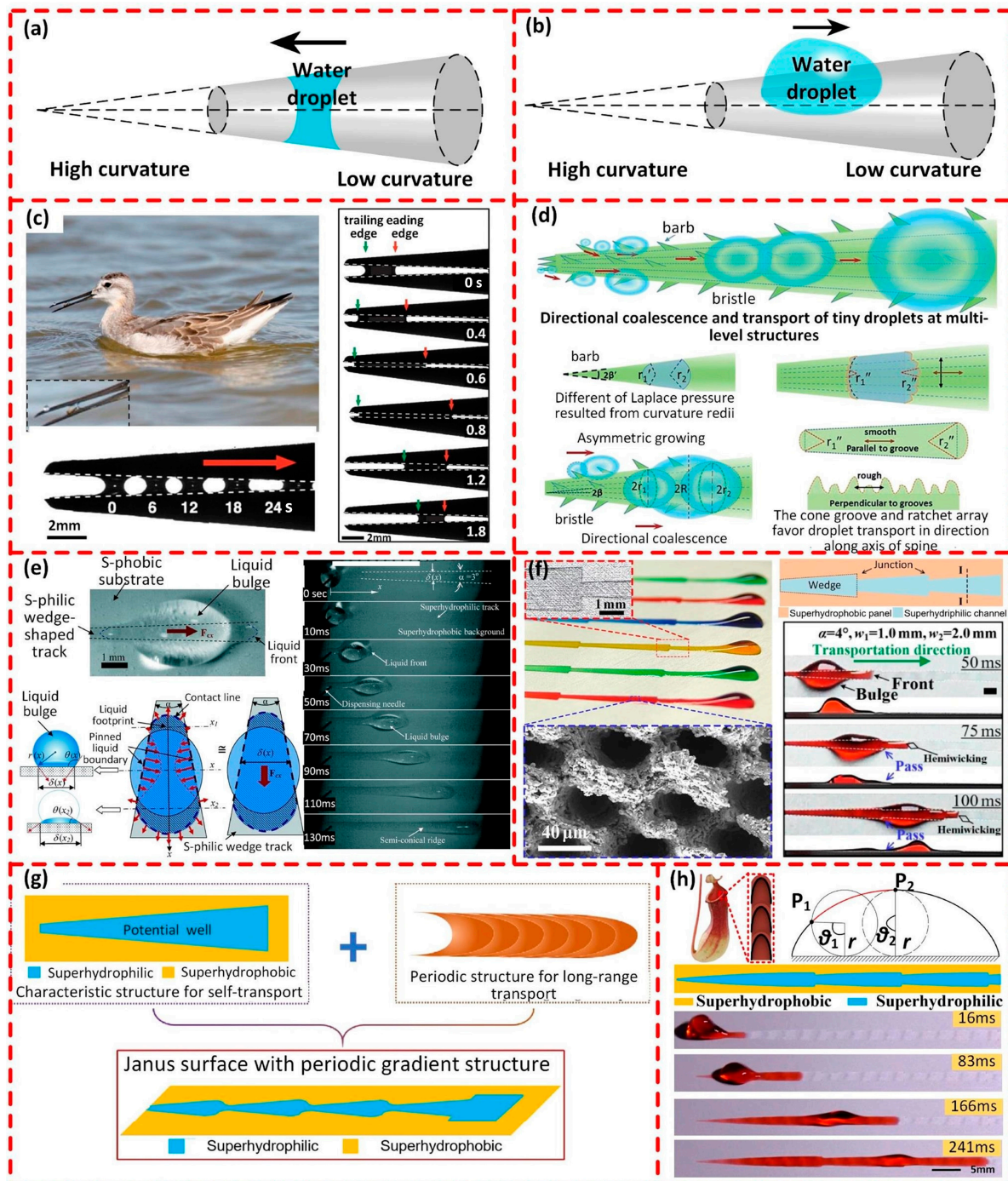
Figure 4. SDWT based on a cone-like shape. (**a**) Schematic illustration of SDWT on the inner surface of the cone. (**b**) Schematic illustration of SDWT on the outer surface of the cone. (**c**) SWDT between asymmetric plates of a shorebird's beak. Reproduced with permission from [57], Copyright 2008, *Science*. (**d**) SDWT on the surface of green bristlegrass bristle. Reproduced with permission from [63], Copyright 2014, *RSC Adv.* (**e**) Force conditions and water droplet motion of SWP. Reproduced with permission from [72], Copyright 2014, *Lab Chip*. (**f**) SDWT on SSWP. Reproduced with permission from [74], Copyright 2022, *Chemical Engineering Journal*. (**g**) Schematic illustration of wedge junction transition optimization. Reproduced with permission from [75], Copyright 2022, *Small Methods*. (**h**) Schematic illustration of SSCP and SDWT on it. Reproduced with permission from [77], Copyright 2023, *Nanoscale*.

3.2.2. Repetitive Array Structure

With the development of SDWT, researchers not only focused on the study of macroscopic wedge shapes but also noticed that water droplets can also transport spontaneously on the surfaces of some plants and animals that do not have apparent shape characteristics. To find the reason for this, they began to focus on the microscopic images of plant and animal surfaces and discovered that these surfaces with repetitive array structures were also capable of water transportation.

In 1990, Sherbrooke [80] found that the special skin of lizards living in desert areas could collect water in a rainy season and could transport water to the mouth in priority. Comanns [81] and his team studied the microstructure on the skins of three different lizards and found that there were honeycomb structures on their skin, which could be used to collect water. The water transportation on the scales of the desert horned lizard was most apparent. Thus, the team imitated this biological structure and fabricated repetitive array structures on polymethyl methacrylate (PMMA) using laser etching technology. As shown in Figure 5a, they made SDWT on this surface possible through a combination of mathematical modeling analysis and experimentation [82–84]. This structure used the asymmetric capillary structure to transport water and used interconnections to make the water droplet form a free liquid surface again so that the next cycle of transportation could be performed.

Not only the skins of animals but also the surface of plants can transport droplets because of the repetitive array structure. The nepenthes plant has a specially evolved leaf for attracting, capturing, and digesting arthropods. Bohn [85] found that there were smooth, overlapping cells on the peristome surface of nepenthes, which allowed the peristome surface to be completely wetted by the rainwater and nectar it secreted. Chen et al. [26] found that the special multilevel asymmetric structure on its peristome surface enhanced capillary action, allowing continuous SDWT and anti-gravity transportation. As shown in Figure 5b, during transportation, the lower layer of water would continue to fill the cavity of the structure, while the upper layer of water would keep spreading forward on a shallower upper track, and the water in the back would be difficult to diffuse backward because of the pinning force generated at the tip of the structure. Based on the above theory, the team fabricated a tilted arch array structure with sharp edges using photolithography to achieve the directional diffusion of water droplets [86–88]. Similarly, Li et al. [89,90] designed a unique topological diode. They used the excess surface energy generated from a water droplet to drive it to break through the front contact line pinning and used the large pinning force to prevent the droplet from being transported backward. This method could achieve fast, long-distance directional transportation, and has good application prospects. However, such array structures are often damaged by external forces, affecting their lifetime. Geng et al. [91] developed a two-dimensional asymmetric pattern to achieve unbalanced forces by controlling the length of the contact line between the water droplet and the hydrophobic pattern, as shown in Figure 5c, which finally resulted in SDWT. Shang et al. [27] were also inspired by nepenthes and found that tilted cone arrays could also be used for SDWT. The use of tilted cone arrays for transportation was also found on araucaria leaf by Feng et al. [92]. These leaves have a specific curvature and cross-arrangement, as shown in Figure 5d, which allows SDWT in three dimensions. Inspired by pine needles, Feng et al. [93] designed asymmetric Janus pillars. As shown in Figure 5e, droplet merging occurs at the tip of the pillars, transforming excess surface energy into kinetic energy, and allowing droplet transportation along the pillars.
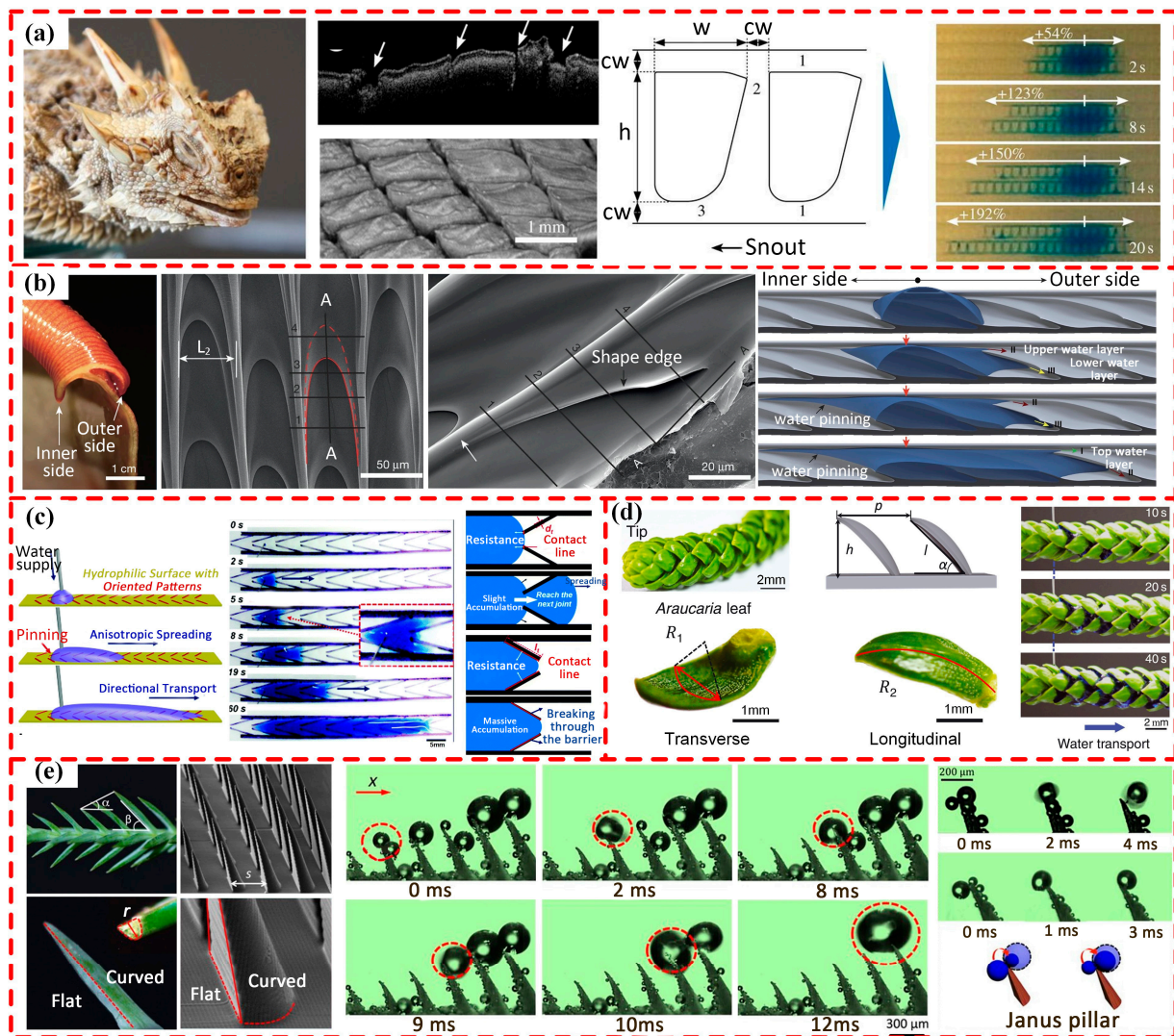
Figure 5. SDWT based on a repetitive array structure. (**a**) The microstructure of the lizard skin and SDWT on a surface inspired by it. Reproduced with permission from [82], Copyright 2015, *Journal of The Royal Society Interface*. (**b**) Continuous SDWT and anti-gravity transportation on the peristome surface of nepenthes. Reproduced with permission from [26], Copyright 2016, *Nature*. (**c**) SDWT on a two-dimensional asymmetric pattern. Reproduced with permission from [91], Copyright 2018, *Materials Horizons*. (**d**) Three-dimensional capillary ratchet-induced SDWT on an araucaria leaf. Reproduced with permission from [92], Copyright 2021, *Science*. (**e**) Droplet-bouncing transportation inspired by pine needles. Reproduced with permission from [93], Copyright 2020, *Sci Adv.*

Summarizing the above methods of using repetitive array structure for SDWT, it can be found that they are all aimed at creating asymmetric force on water droplets by using specially designed structures. The pinning force plays a key role in the transportation process. Through the reasonable design of asymmetric sharp edges, it can only increase the pinning force on just one side of the droplets, which prevents the water droplet from being transported backward. However, this method has a low transportation speed and a loss of water because the droplets are diffused on the surface rather than moving as a whole and are too complex to be fabricated on a large scale.

3.3. SDWT Based on Cooperated Gradient

In nature, many plants and animals do not just use a single transportation method but combine both to achieve more efficient water droplet transportation. SDWT based on

the cooperated gradient is a combination of both wettability gradient and shape gradient, bringing out the strengths of both methods.

In 2010, Zheng et al. [65] found that the spindle knots of spider silk could lead to unbalanced Laplace pressure after studying the water collection processes on Uloborus walckenaerius, as shown in Figure 6a. At the same time, they discovered that spider silk had a wettability gradient due to the difference in the microstructure and shape gradient of the silk. These two factors eventually led to the efficient water collection of spider silk. Meanwhile, polymer-based membranes have been developed in the fields of promoting osmotic energy conversion and droplet-triboelectric nanogenerators due to their excellent mechanical properties, controllable dimensions, and other advantages [94–96]. Inspired by the above, this team fabricated bioinspired bead-on-string silkworm silk using a polymer combined with silkworm silk. They dipped natural silkworm silk (NSS) into a solution of PVDF (poly(vinylidene uoride) in DMF (N,N-dime-thylformamide). The polymer solution film broke up along the NSS to form periodic polymer droplets and formed a periodic spindle structure after phase separation. Due to the good biocompatibility of PVDF, it formed a regular geometrical structure on BSS and had better water collection performance and mechanical properties [97]. Analysis of rapid fog collection on the surface of cactus spines was carried out by Ju et al. [21] This study found that cactus stems were covered by lots of cone-like spines and trichomes and there were multistage microgrooves on the surface of cactus spine. The cone-like shape produced the difference in Laplace pressure, and the microgrooves were sparser near the roots, leading to differences in roughness and then forming a wettability gradient. As shown in Figure 6b, the above two characteristics led to cooperative water transportation. Deng et al. [98] combined a wettability gradient with a single wedge-shaped wettability pattern, which allowed for water droplet transportation on an upside-down surface. Liu et al. [76] also solved the problem of the block caused by the pinning force on SSWP in this way. Chen et al. [99] found in their observations of sarracenia that there are unique hierarchical microchannels on the trichome, as shown in Figure 6c. Two neighboring high ribs formed a large channel that contained 1–5 low ribs, which led to a water film on it. This structure allowed ultrafast SDWT at a speed that was three times faster than that on spider silk and cactus thorn. Combining multiple structures from nature allowed for more efficient SDWT. Park et al. [66] proposed a slippery asymmetric bump by combining the wettability gradient on the back of the beetle, a wedge-shaped pattern of cactus thorn, and the microstructure of the nepenthes. This bump increased the rate of droplet formation during fog collection by six times and greatly improved fog collection efficiency. To solve the unnecessary pinning effect at the contact line, Feng et al. [67] developed a continuous, directional, and long-distance transportation system for fog droplets on the surface of serial cones, as shown in Figure 6d, inspired by spider silk and butterfly wings. Droplets can periodically shift between convex–continuous and concave–intermittent, allowing them to gather at the junction.

Summarizing the above studies, SDWT based on cooperative gradient usually has a faster transportation speed and can also solve the problems of wettability gradient and shape gradient, such as the pinning force at the junction and loss of water. This allows it to be used for fog collection, lab-on-a-chip, and so on. But there are still some limitations, such as the complex fabrication processes and the fixed transportation route.
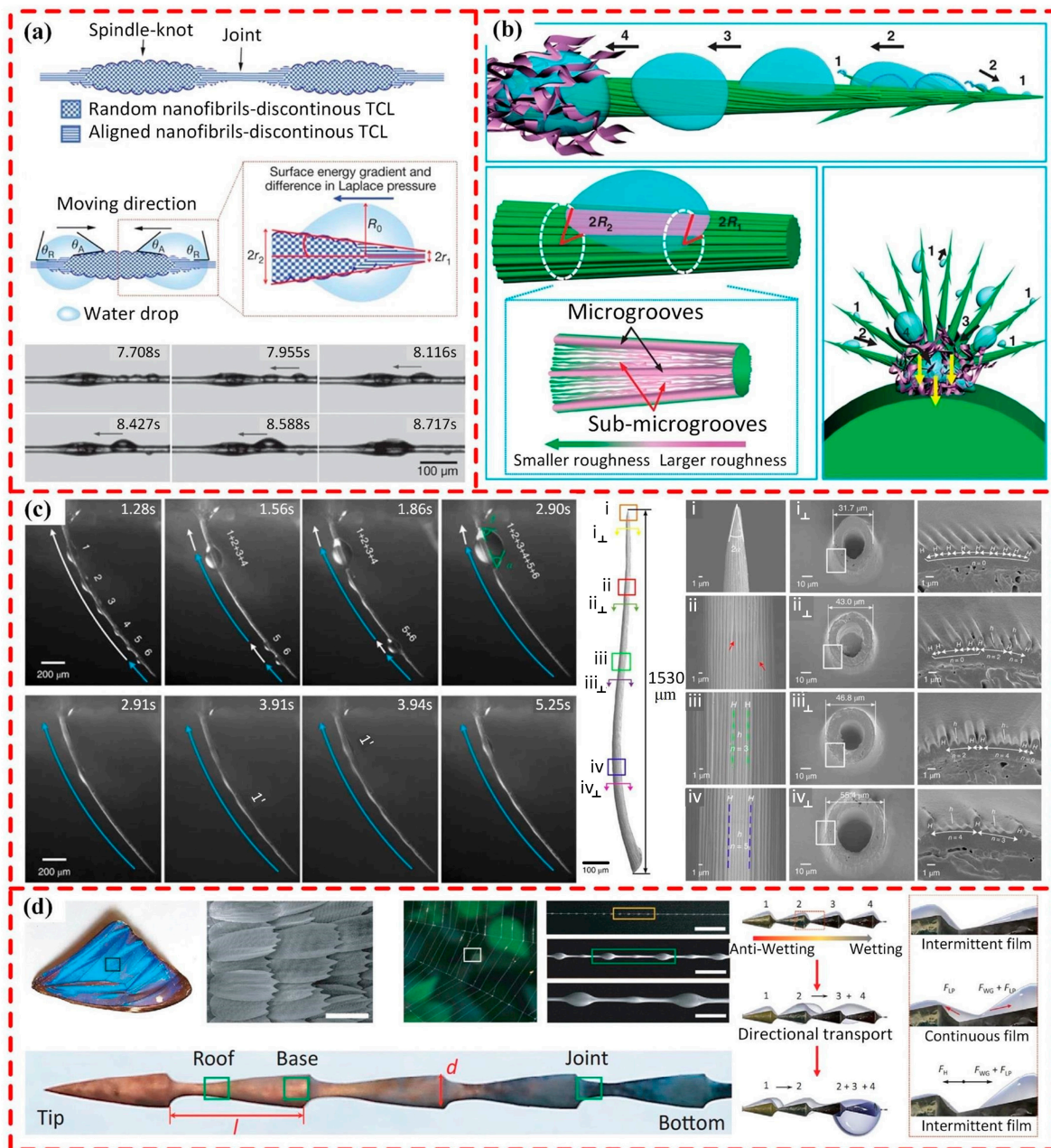
Figure 6. SDWT based on cooperated gradient. (**a**) SDWT due to shape gradients and wettability gradients on spider silk. Reproduced with permission from [65], Copyright 2010, *Nature*. (**b**) SDWT induced by wettability gradient, microgrooves, and cone-shaped structures on cactus surfaces. Reproduced with permission from [21], Copyright 2012, *Nature Communications*. (**c**) Ultra-fast SDWT on the trichome of sarracenia trichome due to the unique hierarchical microchannels and cone-shaped structures. Reproduced with permission from [99], Copyright 2018, *Nature Materials*. (**d**) Continuous, directional, and long-distance transportation on the surface of serial comics inspired by spider silk and butterfly wings. Reproduced with permission from [67], Copyright 2020, *Advanced Materials Interfaces*.

3.4. Applications of SDWT

Through the above sections, we summarized various methods of the SDWT and their principles. Table 1 shows an overview of the characteristics of different transportation strategies. These spontaneous water transportation technologies have a wide range of applications, such as fog collection in dry areas, droplet control in lab-on-a-chip devices, and heat transfer.

Table 1. Summary of different strategies of SDWT.

Classification		Mechanism	Transport Speed	Transport Distance	Fabrication	Robustness
Wettability gradient	Wettability gradient caused by surface composition	Different contact angle, advancing angle, and receding angle	0.5 mm/s–6 mm/s [44] 0.7 mm/s [45] 40 µm/s [46]	7 mm [45] 2.5 mm [46]	Normal	Unstable
	Wettability gradient caused by surface roughness	Different contact angle, advancing angle, and receding angle	5 mm/s–14.6 mm/s [52] 46 mm/s–75 mm/s [53]	3.2 mm–5.2 mm [53]	Complex	Stable
Shape gradient	Cone-like shape	Unbalanced Laplace force	100 mm/s [64] 400 mm/s [72] 289 mm/s [77]	20 mm [72] 50 mm [77]	Simple	Normal
	Repetitive array structure	Unbalanced Laplace force; Principle of minimum surface energy	78 ± 12 mm/s [26] 0.1 mm/s–10 mm/s [82] 1 mm/s–100 mm/s [89]	10–20 mm [26] 20 mm [82]	Complex	Stable
Cooperated gradient	Cooperated gradient	Unbalanced Laplace force; Principle of minimum surface energy; Different contact angle, advancing angle, and receding angle	116.7 mm/s [22] 11.738 mm/s [99] 92 mm/s [76]	5 mm–20 mm [99] 103 mm [76]	Complex	Stable

Freshwater scarcity was a worldwide problem restricting human development. As early as 1992, fog collection was realized on a surface with a wettability gradient by Chaudhury [41]. However, due to the complexity of its fabrication and low collection efficiency, researchers started to focus on other methods. They successively found fog collection phenomena on the backs of beetles [19], spider silk [65], and cactus spines [21,97] and were inspired by them. Xu et al. [100] proposed a mixed-surface film by adding hydrophobic Ag and hydrophilic nano TiO_2 to a bio-based film. Its fog collection rate is as high as 1043 mg·cm^{-2}·h^{-1}. Inspired by cactus, Ju et al. [101] also achieved efficient fog collection using cone-like copper wires with a wettability gradient. To solve the limitation of low droplet shedding efficiency, Zhou [23] developed a proposal that combined the structure of the cactus spine and Janus membrane. This proposal used a cone-like shape structure with microstructure to collect the fog and transport the water droplets. Then, the Janus membrane was placed vertically to the cone to collect water droplets. This study realized continuous water collection. Due to the small size of the cone surface, researchers designed a star-shaped pattern on a flat surface to achieve more efficient fog collection [102]. The fog collection reached 2780 mg/cm^{-2}·h^{-1} when the surface was tilted 45°. But it had a limitation in that it could not collect the droplets created by fog collection if the surface was parallel to the ground. To solve this limitation, Wu et al. [103] designed a snowflake-like pattern with a small hole, as shown in Figure 7a. The droplet could spontaneously transport to the hole by Laplace pressure and then be collected by the hole with a wettability gradient. In addition, Yan et al. [104] designed a super-fast fog collector based on the Laplace pressure difference generated by a miniature fog droplet on a superhydrophobic surface with a

superhydrophilic pore and developed a theory model of fog collection efficiency. The collection rate and efficiency of this super-fast fog collector were as high as 4.21 g·cm^{-2}·h^{-1} and 35.68%, respectively.

Droplets of different compositions have different transportation motions on the same surface. So, researchers can use this theory to realize the spontaneous separation of mixed liquids. Feng et al. [105] developed a superhydrophobic and superoleophilic coating mesh film. Because of the different wettability between the two sides of the pore, oil and water could be separated. Li et al. [106] fabricated an asymmetric repetitive array structure by imitating the peristome surface of nepenthes. These structures drove the oil droplet transport spontaneously and prevented water droplet transportation. This team designed a device that can separate small oil droplets mixed in water, as shown in Figure 7b.

SDWT has gradually become a focus in the field of microfluidics due to its advantages of no external excitation, fast mixing speed [78,79], and low cross-contamination. Shang et al. [27] proposed an artificial nepenthes peristome by controlling the magnetic field to tilt the cone array. This surface allowed the mixture of various kinds of water, as shown in Figure 7c. The potassium permanganate and ascorbic acid from different paths mixed spontaneously, causing the potassium permanganate to gradually lose its distinctive dark-purple color because it was reduced by ascorbic acid. Yang et al. [107] fabricated a hydrophilic track with a certain angle on a superhydrophobic aluminum surface. This pattern not only could mix the liquid but also could grab and release water droplets, providing a new idea for water droplet control in lab-on-a-chip devices.
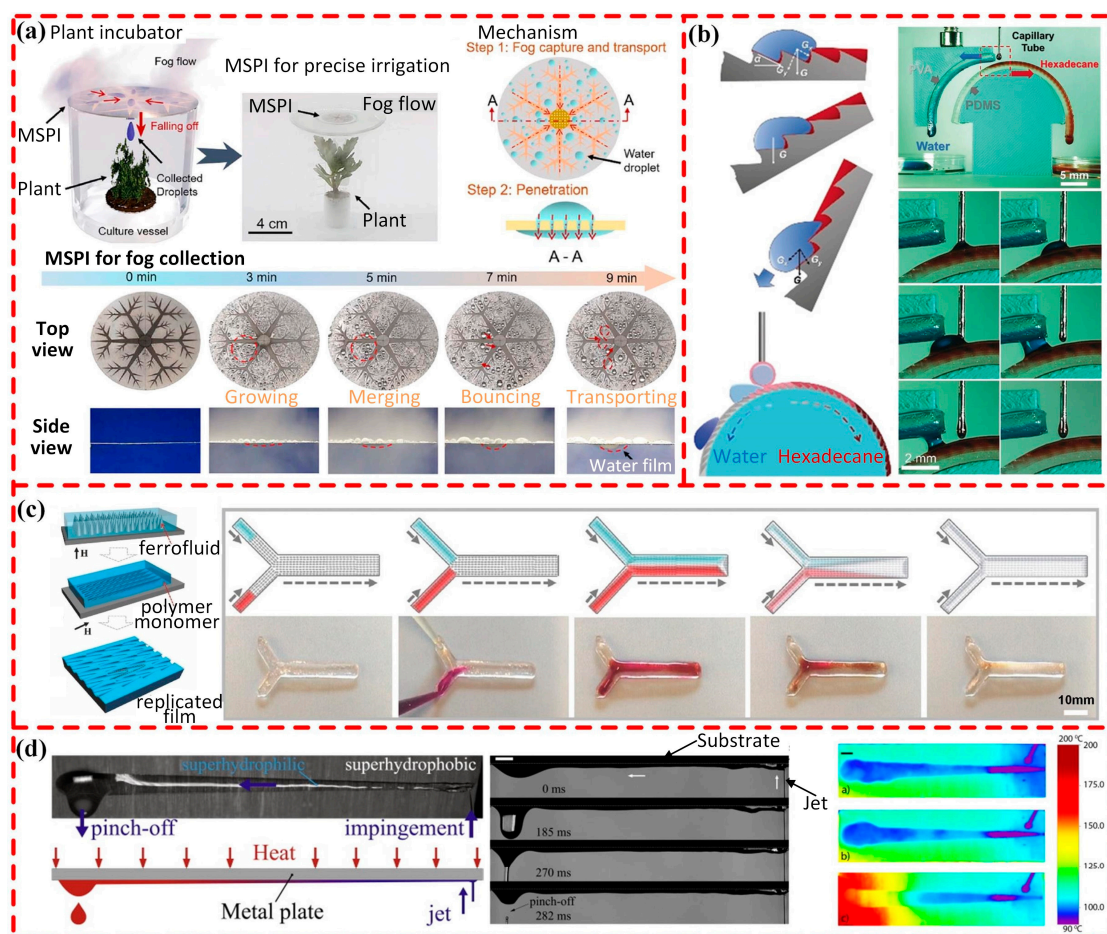

Figure 7. Applications of the SDWT. (**a**) Flog collection on a snowflake-like pattern. Reproduced with permission from [103], Copyright 2023, *Journal of Materials Chemistry A*. (**b**) Separation of oil and

water on ratchet construction inspired by the nepenthes. Reproduced with permission from [106], Copyright 2017, *Angew. Chem. Int. Ed*. (**c**) The mixture of various kinds of liquid based on the SDWT. Reproduced with permission from [27], Copyright 2018, *Advanced Functional Materials*. (**d**) Directionally controllable water jet cooling system. Reproduced with permission from [108], Copyright 2016, *International Journal of Heat and Mass Transfer*.

SDWT also can be used in the field of heat transfer. Koukoravas et al. [108] designed a heat transfer device, as shown in Figure 7d. Water jets were injected from the narrow side of the wedge. Then, the water was transported to the wide side against gravity and then dropped. This process took away the heat generated by the heating source. Compared with conventional jet cooling, this method could provide a cooling effect that was about four times better and used less coolant. The team also studied the shape of the tracks and designed a multi-track cooling device that had a thermal removal rate of 100 W/cm^2 when the coolant flow rate was 1 m/s and the chip was overheated by 65 °C [109].

The above applications of SDWT have had a positive impact on environmental impact and sustainability. The applications related to fog collection play a role in environmental protection and the water cycle. Such functional surfaces can help to realize the collection of water resources in desert areas, which can be used to irrigate vegetation and promote the water cycle in the desert in order to combat desertification. Wastewater treatment often requires the use of environmentally harmful chemicals. The use of super-wetted surfaces for the separation of oil–water mixtures provides a new idea for wastewater treatment. On the one hand, it can enhance the utilization of water resources, and on the other hand, it can reduce waste and pollution. More importantly, since these functional surfaces work without the input of external energy, they also help to save energy.

4. Spontaneous Directional Transportation of Gas Bubble (SDBT): Methods and Applications

Researchers found that superhydrophobic surfaces exhibited underwater superaerophilic properties, and superhydrophilic surfaces exhibited underwater superaerophobic property underwater. Based on the above phenomena, they fabricated surfaces with gradient characteristics to achieve the underwater SDBT. The gradient characteristics used for SDBT can be divided into three types: wettability gradient, shape gradient, and cooperate gradient.

4.1. SDBT Based on Wettability Gradient

The Janus membrane is a typical surface with a wettability gradient. Yan et al. [110] fabricated a Janus aluminum foil membrane with a water contact angle of 23° on one side and a water contact angle of 155° on the other side using laser processing. As shown in Figure 8a, the gas bubble would continuously transport to the superhydrophobic upper surface (superaerophilic surface) when contacting the hydrophilic lower surface (aerophobic surface). In the opposite direction, the gas bubbles were blocked, resulting in SDBT. Huo et al. [111] fabricated a stainless steel mesh with similar properties that enabled the interception, penetration, and collection of underwater gas bubbles. It also could be used for the elimination and collection of gas bubbles in containers. Dai et al. [112] used UV radiation technology to modulate the wettability of the TiO$_2$-sprayed copper foam surface. They found that the difficulty of gas bubble penetration depended on the difficulty of their transition from gas–liquid contact to gas–solid contact. When the hydrophilic surface had continuous water film adsorption, the upward penetration of the gas bubble became more difficult. In addition, researchers also fabricated a wettability gradient on non-metallic materials and conducted SDBT on it. Hou et al. [113] fabricated a Janus membrane for the transportation and collection of underwater gas bubbles on a PDMS substrate with an underwater contact angle of 156° on one side and an underwater contact angle of 0° on the other side. Inspired by fish scales and lotus leaves, Yong et al. [114] fabricated a wettability gradient on a silicon wafer to achieve the capture and collection of gas bubbles, as shown in Figure 8b. Tahzibi et al. [115] also achieved fast capture, collection, and directional transportation of underwater gas bubbles on a Janus carbon cloth. Yin et al. [116] fabricated

a Janus membrane by constructing a wettability gradient on polytetrafluoroethylene (PTFE) using laser processing. On this surface, gas bubbles could transport directionally from the aerophobic side to the aerophilic side of the Janus membrane.
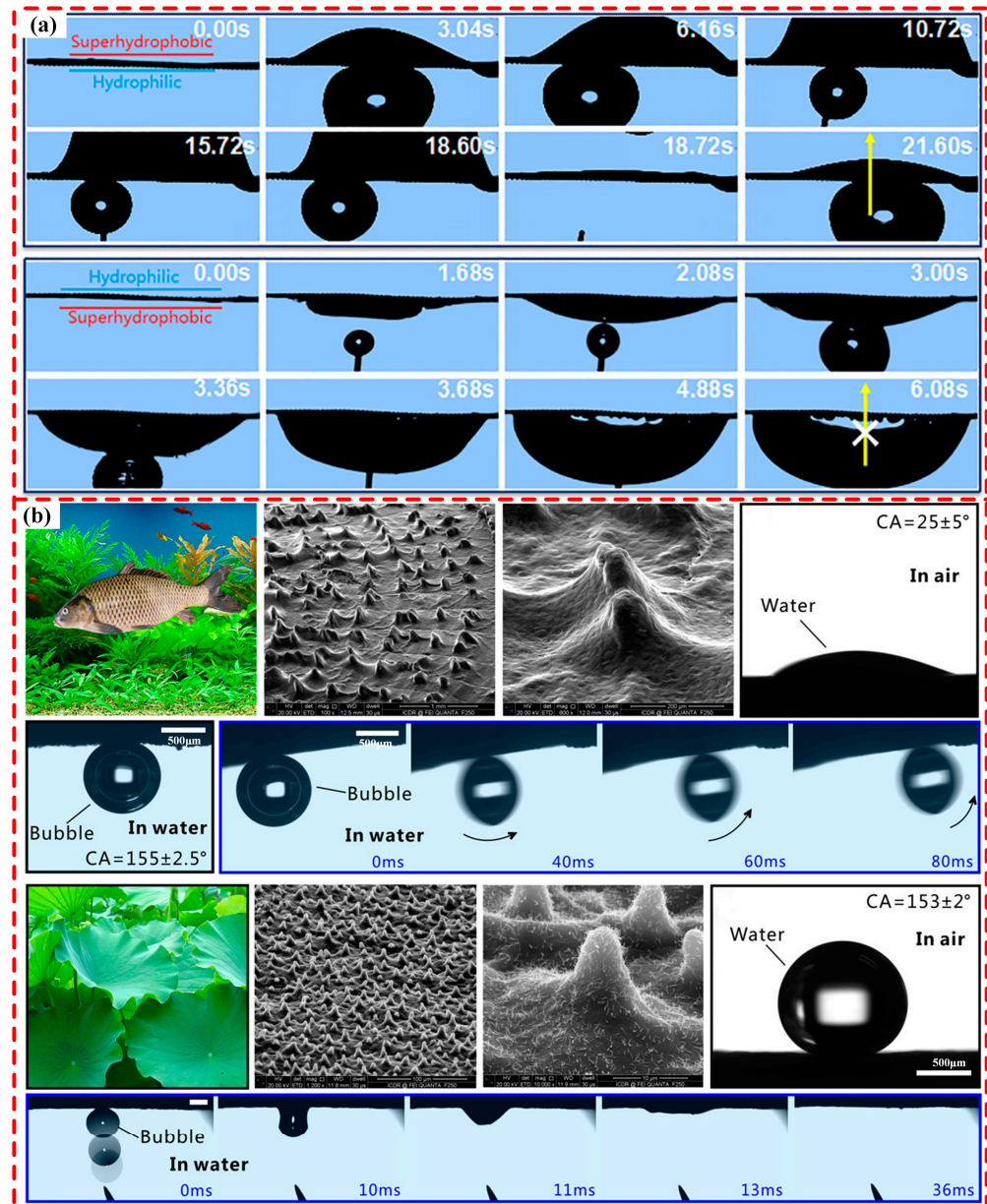

Figure 8. Underwater SDBT based on wettability gradient. (**a**) SDBT on Janus membrane. Reproduced with permission from [110], Copyright 2018, *Applied Physics Letters*. (**b**) Bubble capture and collection on biomimetic silicon wafer surface. Reproduced with permission from [114], Copyright 2017, *ACS Applied Materials & Interfaces*.

4.2. SDBT Based on Shape Gradient

There are two main types of shape gradient for spontaneous directional gas bubble transportation: the structural gradient between two neighboring gas bubbles and the cone-like shape gradient.

4.2.1. The Structural Gradient between Two Neighboring Gas Bubbles

Due to the Laplace force generated by the different sizes of the two gas bubbles, the small gas bubble will spontaneously transport towards the large one along the track. Yong

et al. [117] fabricated superhydrophobic regions of different sizes on PTFE using laser etching technology. When the sample was placed underwater, it can be found that the gas bubble was able to transport spontaneously from the small region to the large region because the gas bubble captured by a small superaerophilic pattern is also smaller than that of the large one. Xie et al. [118] fabricated a dumbbell-like pattern with two regions of different sizes in order to realize the SDBT. They found that the different surface energy between the starting and ending points drove the directional transportation of the gas bubble. In other words, a gas bubble could transport spontaneously from the small region to the large region and eventually separate from the surface by buoyancy. However, the gas bubble could not transport spontaneously in the opposite direction, as shown in Figure 9a,b.

4.2.2. Cone-like Shape

Yu et al. [119] were the first to apply the shape gradient to the underwater SDBT and found that a superaerophilic copper cone can capture gas bubbles effectively. The gas bubble was driven by the different Laplace pressure between the narrow side and the wide side of the cone, which makes the gas bubble transport from the tip to the root of the cone, as shown in Figure 9c. In addition, it was also found that the superaerophilic copper cone could capture gas bubbles effectively due to the existence of an air film, while the superaerophobic surfaces were infiltrated by the water and could not capture gas bubbles. Xiao et al. [120] studied the gas bubble transportation ability on the aerophilic cone in a low-surface-energy medium and showed that the aerophilic cone was still able to control bubbles easily in such a medium (29.9 mN/m) at a temperature of 20 °C. Xue et al. [121] found that in a supersaturated CO_2 solution, the neighboring bubbles could merge on the surface of a cone and could transport to the root of it spontaneously. Considering the limited transportation distance of a single cone-like shape, Jiang et al. [122] used a spiral structure to achieve long-distance transportation of gas bubbles, but it was necessary to shake the spiral structure to make the gas bubble transport. To solve this problem, Shi et al. [123] combined the spiral structure with a cone-like shape, which achieved a long transportation distance, as shown in Figure 9d.

In 2017, Yu et al. [124] processed the polyethylene substrate into a wedge shape by laser etching, which realized underwater SDBT by using a 2D wedge-shaped pattern for the first time, as shown in Figure 9e. The high driving force provided by the wedge-shaped pattern and the low drag force formed by the superaerophilic enabled SDBT. It was also possible to transport gas bubbles in complex conditions, such as on an S-shaped surface, helical surface, and bi-gradient surface. Liu et al. [125] then pre-covered the superaerophilic wedge-shaped pattern with air film, as shown in Figure 9f, to achieve a faster transportation speed. This method extended transportation distances by 14.12% and increased the transportation speed by 24.29% compared to that without air film. To solve the problem of the short transportation distance of a single superaerophilic wedge-shaped pattern, as shown in Figure 9g, Song et al. [126] designed a serial superaerophilic wedge-shaped pattern. By changing the parameters of the pattern, it was possible to control the "passing" and "blocking" states of the bubble at the junction. This method also could realize the long-distance transportation of gas bubbles underwater.
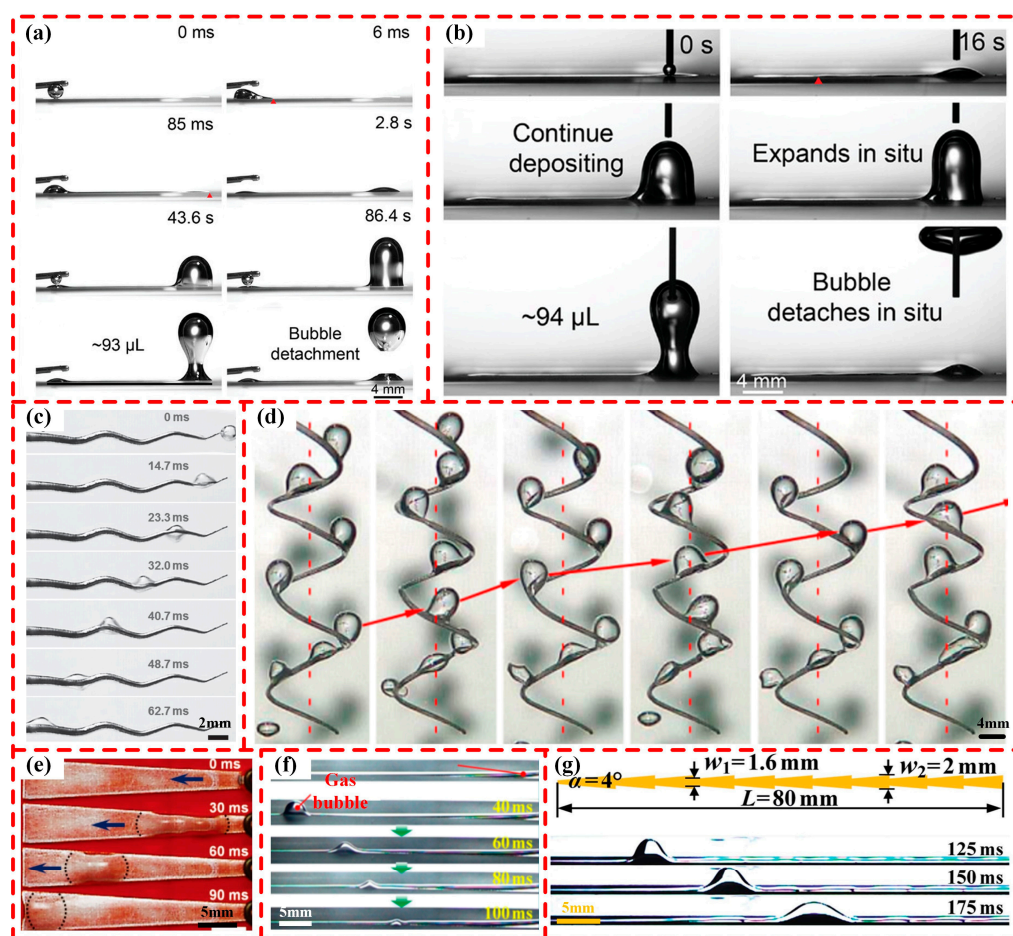
Figure 9. SDBT based on shape gradient. (**a**,**b**) SDBT caused by Laplace pressure generated from two neighboring gas bubbles. Reproduced with permission from [118], Copyright 2023, *Advanced Materials*. (**c**) SDBT on superaerophilic cones underwater. Reproduced with permission from [119], Copyright 2016, *Advanced Functional Materials*. (**d**) Underwater bubble transport process on a spiral structure. Reproduced with permission from [123], Copyright 2020, *ACS Applied Materials & Interfaces*. (**e**) Underwater SDBT on a wedge-shaped pattern. Reproduced with permission from [124], Copyright 2017, *Advanced Functional Materials*. (**f**) SDBT on wedge-shaped pattern with pre-covered air film. Reproduced with permission from [125], Copyright 2019, *ACS Applied Materials & Interfaces*. (**g**) Underwater SDBT on superaerophilic serial wedge-shaped pattern. Reproduced with permission from [126], Copyright 2019, *Journal of Materials Chemistry A*.

4.3. SDBT Based on Cooperated Gradient

To achieve better transportation properties, researchers have combined shape gradient with wettability gradient to form multifunctional transportation. Inspired by the surfaces of natural plants and animals such as cacti, water spiders, and lotus leaves, Jiang et al. [127] fabricated foam electrodes with a cooperated gradient. Gas bubbles would spontaneously transport from the narrow side to the side of the electrode due to the wettability gradient and shape gradient, which achieved cooperative transportation. This method can be used in water electrolysis experiments to separate and collect oxygen and hydrogen, as shown in Figure 10a,b.

The SDBT on cooperative surfaces has more application possibilities than the single-gradient method. In addition, it also performs better than methods that only use a single gradient in terms of gas bubble transportation efficiency. However, the complexity of manufacturing and other issues arising from it still need to be solved.
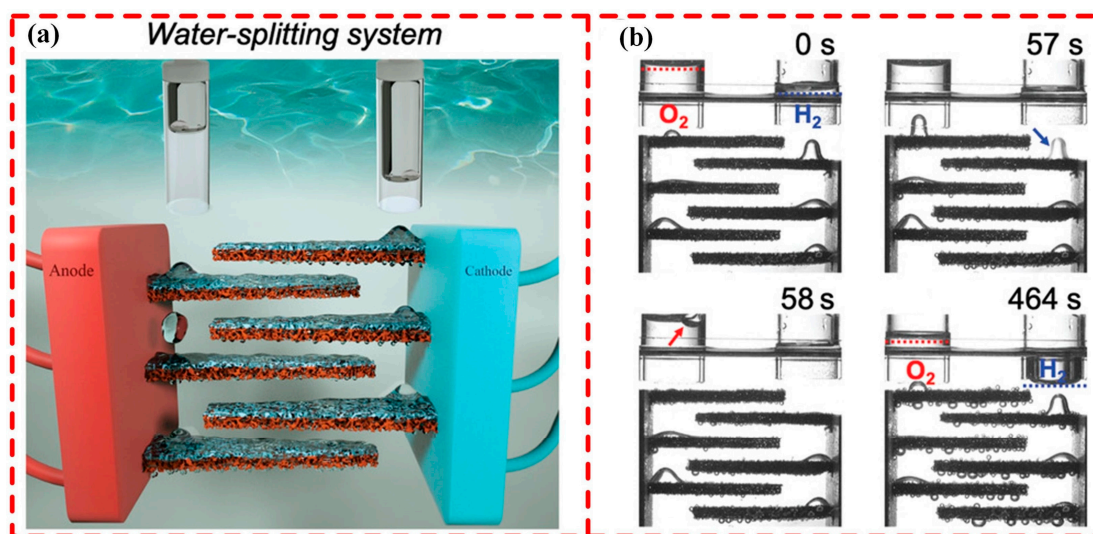
Figure 10. SDBT based on cooperation surfaces. (**a**) Schematic illustration of the water-splitting system. (**b**) Gas separation process. Reproduced with permission from [127], Copyright 2020, *Advanced Materials*.

4.4. Applications of SDBT

Researchers have proposed various patterns such as wedge-like and cone-like shapes to drive gas bubbles underwater based on Laplace pressure. Table 2 shows an overview of the characteristics of different transportation strategies for SDBT. Due to the advantages of spontaneous transportation and simple structure, SDBT driven by surface gradient force has important application prospects in various aspects of daily life and industrial production, such as gas collection, hydrogen precipitation reaction, and underwater sensors.

Table 2. Summary of different strategies of SDBT.

Classification		Mechanism	Transport Speed/ Passing Rate	Transport Distance	Fabrication	Robustness
Wettability gradient	Janus membrane	Different Laplace pressure	0.0259 mL·s^{-1} cm^{-2} [110] 22.2 mL·s^{-1} cm^{-2} [113]	N/A	Normal	Stable
Shape gradient	The structural gradient between two neighboring gas bubbles	Unbalanced Laplace force; Principle of minimum surface energy	350 mm/s–520 mm/s [118]	10 mm [117] 40 mm [118]	Simple	Stable
	Cone-like shape	Unbalanced Laplace force	79.8 ± 4.8 cm/s [119] 327 mm/s [124] 400 mm/s [126]	10 mm–20 mm [119] 80 mm [126]	Simple	Normal
Cooperated gradient	Cooperated gradient	Unbalanced Laplace force; Principle of minimum surface energy	N/A (Too little relevant research)	N/A (Too little relevant research)	Complex	Stable

Environmental protection is an eternal theme for humankind. The release of hazardous gases due to accidents and industrial development exacerbates the greenhouse effect. Therefore, underwater directional gas transportation and collection are especially important for environmental protection. Xiao et al. [128] used the designed 2D superaerophilic surface to transport hydrogen and superaerophilic sponge and tubes to collect gas bubbles, as shown in Figure 11a. Ning et al. [129] also designed an underwater gas bubble collection device that consisted of a single layer of superaerophilic mesh and quartz tubes. This device could be sealed and was able to collect underwater gas bubbles. Gas bubbles also have an important impact on catalytic production, especially in the hydrogen precipitation reaction. If gas bubbles cannot be removed in time, they will attach to the electrode, resulting in insufficient reactions between the electrode and the electrolyte, which affect the production efficiency in the end. Yu et al. [130] fabricated a multifunctional electrode for bubble generation, transportation, and collection by combining a superaerophilic sponge with an aerophilic cone-shaped electrode. The cone-shaped electrode functioned as a reduction electrode to generate hydrogen. The generated hydrogen would transport along the aerophilic surface toward the root where there was a superaerophilic sponge. Once the hydrogen gas touched the superaerophilic sponge, it would be absorbed immediately, which allowed the electrode to have enough area for continued hydrogen precipitation reactions, as shown in Figure 11b.
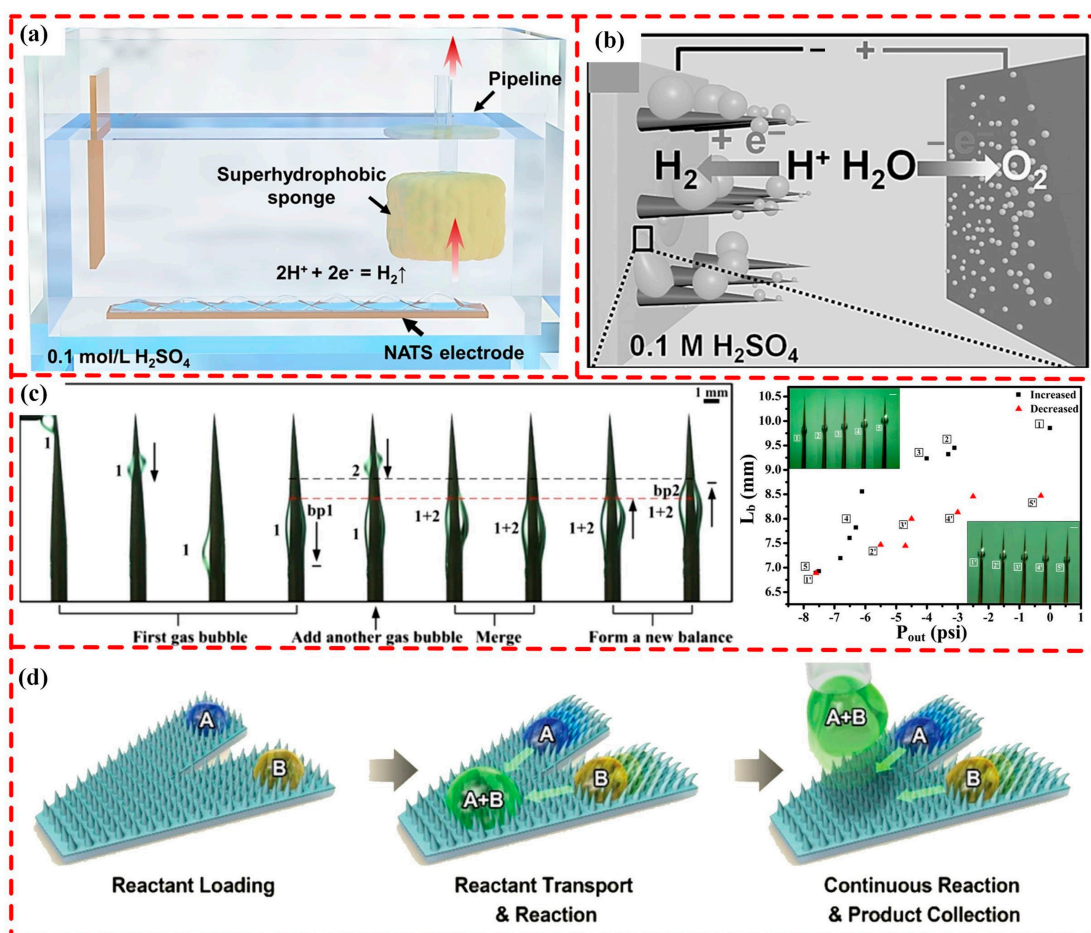

Figure 11. Applications of underwater SDBT. (**a**) Gas collection on a flat electrode. Reproduced with permission from [128], Copyright 2021, *Advanced Functional Materials*. (**b**) Gas transportation and collection on cone-shaped electrodes. Reproduced with permission from [130], Copyright 2016, *Advanced Functional Materials*. (**c**) Monitoring with bubble sensors. Reproduced with permission from [131], Copyright 2018, *ACS Applied Materials & Interfaces*. (**d**) Microbubble reactor. Reproduced with permission from [132], Copyright 2021, *Advanced Functional Materials*.

The control of underwater gas bubbles is flexible and versatile, which not only plays a role in the study of gas collection but also has good application prospects in the field of sensor monitoring. Xue et al. [131] fabricated a superhydrophobic cone by electrochemical etching and found that the equilibrium position of a gas bubble whose volume is a constant value was fixed on the cone. This meant that the equilibrium point could be changed by increasing or decreasing the volume of gas bubbles, as shown in Figure 11c. Thus, this team designed an underwater sensor based on such a theory.

The spontaneous and directional motion property of underwater gas bubbles also provides a new method to conduct chemical reactions. Ma et al. [124] injected hydrogen and oxygen bubbles into two different narrow sides of the pattern. The two gas bubbles transported towards each other along the track and merged at the middle position of the pattern due to the driving of the Laplace pressure. The mixture bubble undergoes a violent combustion reaction upon ignition. Han et al. [132] fabricated a gas bubble microreactor based on a magnetically controlled V-slip surface. The gas bubbles from different areas could transport to each other and eventually merge at the junction to perform a chemical reaction, as shown in Figure 11d.

The applications of SDBT also have a positive impact on the environment and sustainability. Since a well-designed SDBT surface can help to reduce the drag force of ships under water, energy can be saved. In the field of marine antifouling, SDBT can help prevent the corrosion of deep-sea instruments. Since it can realize the spontaneous directional transportation of underwater air bubbles, it can create the air film without energy input to isolate seawater and achieve corrosion prevention of instruments.

5. Conclusions and Perspectives

Spontaneous directional transportation (SDT) of water and gas opens up a new venue for the new high-performance fluid transportation system. In this review, we first introduced the important basic theories related to fluid transportation, then reviewed and discussed the related methods and limitations of spontaneous directional water droplet transportation (SDWT) and spontaneous directional gas bubble transportation (SDBT), and finally summarized and reviewed the latest progress of the SDWT and the SDBT in practical applications. Although significant progress has been made, there are still many directions that need to be further investigated. First of all, their control accuracy of transportation is not high; due to the absence of external force, the precise control of droplets (such as the start/stop time and speed control in the process of transportation) is a major difficulty, and SDT remains a certain technology gap in the field of programmable chips. In addition, the fabrication processes of SDWT and SDBT are complex and expensive, which means that the transition from laboratory research to practical applications remains a challenge. Furthermore, the SDT surface may lose superhydrophobicity/superhydrophilicity after the impact or friction, which leads to the invalidation of the SDT surface. Therefore, it is important to develop a highly robust SDT surface that can be used in harsh environments. Moreover, for both SDWT and SDBT, the transportation speed is not fast enough. The fast transportation speed of water droplets and gas bubbles can further improve the condensate water collection efficiency of the life-support system of the manned space station, enhance the cooling efficiency of spacecraft electronics, and increase the drag reduction capacity of ship micro-bubbles. In addition, the current theoretical studies on SDTs are mainly focused on qualitative approaches such as force analysis. Quantitative relationship models between structural parameters and motion behavior (conveying speed, distance, etc.) may need more in-depth research.

Author Contributions: Conceptualization, Y.L. and D.Y.; investigation, Y.L., J.L. and S.Z.; resources, J.S.; writing—original draft preparation, Y.L., J.L. and S.Z.; writing—review and editing, Y.L., D.Y. and J.S.; supervision, J.S. All authors have read and agreed to the published version of the manuscript.

Institutional Review Board Statement: Not applicable.

Informed Consent Statement: Not applicable.

Data Availability Statement: Not applicable.

Conflicts of Interest: The authors declare no conflict of interest.

References

1. Tian, X.; Verho, T.; Ras, R.H.A. Moving superhydrophobic surfaces toward real-world applications. *Science* **2016**, *352*, 142–143. [CrossRef]
2. Zhao, W.; Jiang, Y.; Yu, W.; Yu, Z.; Liu, X. Wettability Controlled Surface for Energy Conversion. *Small* **2022**, *18*, 2202906. [CrossRef]
3. Wang, L.; Zhao, H.; Zhu, D.; Yuan, L.; Zhang, H.; Fan, P.; Zhong, M. A Review on Ultrafast Laser Enabled Excellent Superhydrophobic Anti-Icing Performances. *Appl. Sci.* **2023**, *13*, 5478. [CrossRef]
4. Yang, X.; Zhuang, K.; Lu, Y.; Wang, X. Creation of Topological Ultraslippery Surfaces for Droplet Motion Control. *ACS Nano* **2021**, *15*, 2589–2599. [CrossRef]
5. Pan, W.; Wang, Q.; Ma, J.; Xu, W.; Sun, J.; Liu, X.; Song, J. Solid-Like Slippery Coating with Highly Comprehensive Performance. *Adv. Funct. Mater.* **2023**, *33*, 2302311. [CrossRef]
6. Zhang, L.; Rokshana, P.; Yu, Y.; Zhao, Y.; Ye, F. Near-Infrared Responsive Droplet for Digital PCR. *Small* **2022**, *18*, 2107858. [CrossRef]
7. Yang, S.; Li, M.; Li, C.; Yan, L.; Li, Q.; Gong, Q.; Li, Y. Droplet-Driven Self-Propelled Devices Fabricated by a Femtosecond Laser. *ACS Appl. Mater. Interfaces* **2023**, *15*, 36899–36907. [CrossRef]
8. Dorvee, J.R.; Derfus, A.M.; Bhatia, S.N.; Sailor, M.J. Manipulation of liquid droplets using amphiphilic, magnetic one-dimensional photonic crystal chaperones. *Nat. Mater.* **2004**, *3*, 896–899. [CrossRef]
9. Timonen, J.V.I.; Latikka, M.; Leibler, L.; Ras, R.H.A.; Ikkala, O. Switchable Static and Dynamic Self-Assembly of Magnetic Droplets on Superhydrophobic Surfaces. *Science* **2013**, *341*, 253–257. [CrossRef]
10. Wang, L.; Jiang, G.; Zhu, D.; Tian, Z.; Chen, C.; Hu, X.; Peng, R.; Li, D.; Zhang, H.; Zhao, H.; et al. Self-Driven Droplet Motions Below their Icing Points. *Small* **2023**, 2302339. [CrossRef]
11. Dai, H.; Gao, C.; Sun, J.; Li, C.; Li, N.; Wu, L.; Dong, Z.; Jiang, L. Controllable High-Speed Electrostatic Manipulation of Water Droplets on a Superhydrophobic Surface. *Adv. Mater.* **2019**, *31*, 1905449. [CrossRef]
12. Zhang, Y.; Ming, P.; Xue, B.; Liu, H.; Yang, X.; Li, L.; Niu, S.; Yan, L.; Zheng, X.; Qin, G. Facilely fabricating large-area robust heterogeneous wettability surface by mask-patterned ultrafine anode scanning electrodeposition for efficient water collection. *Surf. Interfaces* **2023**, *41*, 103247. [CrossRef]
13. Sun, Q.; Wang, D.; Li, Y.; Zhang, J.; Ye, S.; Cui, J.; Chen, L.; Wang, Z.; Butt, H.-J.; Vollmer, D.; et al. Surface charge printing for programmed droplet transport. *Nat. Mater.* **2019**, *18*, 936–941. [CrossRef] [PubMed]
14. Liu, C.; Lu, C.; Yuan, Z.; Lv, C.; Liu, Y. Steerable drops on heated concentric microgroove arrays. *Nat. Commun.* **2022**, *13*, 3141. [CrossRef] [PubMed]
15. Wang, Z.; Zhao, Z.; Wen, G.; Zhu, Y.; Chen, J.; Jing, X.; Sun, S.; Zhang, L.; Liu, X.; Chen, H. Fracture-Promoted Ultraslippery Ice Detachment Interface for Long-Lasting Anti-icing. *ACS Nano* **2023**, *17*, 13724–13733. [CrossRef]
16. McGloin, D.; Burnham, D.R.; Summers, M.D.; Rudd, D.; Dewar, N.; Anand, S. Optical manipulation of airborne particles: Techniques and applications. *Faraday Discuss.* **2008**, *137*, 335–350. [CrossRef]
17. Ichimura, K.; Oh, S.K.; Nakagawa, M. Light-driven motion of liquids on a photoresponsive surface. *Science* **2000**, *288*, 1624–1626. [CrossRef]
18. Liu, G.L.; Kim, J.; Lu, Y.; Lee, L.P. Optofluidic control using photothermal nanoparticles. *Nat. Mater.* **2006**, *5*, 27–32. [CrossRef]
19. Parker, A.R.; Lawrence, C.R. Water capture by a desert beetle. *Nature* **2001**, *414*, 33–34. [CrossRef]
20. Wang, Z.; Wang, Y.; Liu, G. Rapid and Efficient Separation of Oil from Oil-in-Water Emulsions Using a Janus Cotton Fabric. *Angew. Chem. Int. Ed.* **2016**, *55*, 1291–1294. [CrossRef]
21. Ju, J.; Bai, H.; Zheng, Y.; Fang, R.; Jiang, L. A multi-structural and multi-functional integrated fog collection system in cactus. *Nat. Commun.* **2012**, *3*, 1247. [CrossRef] [PubMed]
22. Xu, T.; Lin, Y.; Zhang, M.; Shi, W.; Zheng, Y. High-Efficiency Fog Collector: Water Unidirectional Transport on Heterogeneous Rough Conical Wires. *ACS Nano* **2016**, *10*, 10681–10688. [CrossRef] [PubMed]
23. Zhou, H.; Zhang, M.; Li, C.; Gao, C.; Zheng, Y. Excellent Fog-Droplets Collector via Integrative Janus Membrane and Conical Spine with Micro/Nanostructures. *Small* **2018**, *14*, 1801335. [CrossRef] [PubMed]
24. Uddin, M.N.; Rab, M.F.; Islam, A.K.M.N.; Asmatulu, E.; Rahman, M.M.; Asmatulu, R. Nanostructured Hybrid Hydrogels for Solar-Driven Clean Water Harvesting from the Atmosphere. *Materials* **2022**, *15*, 7538. [CrossRef]
25. Lin, F.; Wo, K.; Fan, X.; Wang, W.; Zou, J. Directional Transport of Underwater Bubbles on Solid Substrates: Principles and Applications. *ACS Appl. Mater. Interfaces* **2023**, *15*, 10325–10340. [CrossRef] [PubMed]

26. Chen, H.; Zhang, P.; Zhang, L.; Liu, H.; Jiang, Y.; Zhang, D.; Han, Z.; Jiang, L. Continuous directional water transport on the peristome surface of *Nepenthes alata*. *Nature* **2016**, *532*, 85–89. [CrossRef]

27. Shang, L.; Yu, Y.; Gao, W.; Wang, Y.; Qu, L.; Zhao, Z.; Chai, R.; Zhao, Y. Bio-Inspired Anisotropic Wettability Surfaces from Dynamic Ferrofluid Assembled Templates. *Adv. Funct. Mater.* **2018**, *28*, 1705802. [CrossRef]

28. Jiao, Y.; Lv, X.; Zhang, Y.; Li, C.; Li, J.; Wu, H.; Xiao, Y.; Wu, S.; Hu, Y.; Wu, D.; et al. Pitcher plant-bioinspired bubble slippery surface fabricated by femtosecond laser for buoyancy-driven bubble self-transport and efficient gas capture. *Nanoscale* **2019**, *11*, 1370–1378. [CrossRef]

29. Yan, D.; Wang, Y.; Liu, J.; Zhao, D.; Ming, P.; Song, J. Electrochemical 3D printing of superhydrophobic pillars with conical, cylindrical, and inverted conical shapes. *Colloids Surf. A Physicochem. Eng. Asp.* **2021**, *625*, 126869. [CrossRef]

30. Pan, W.; Wu, S.; Huang, L.; Song, J. Large-Area Fabrication of Superhydrophobic Micro-Conical Pillar Arrays on Various Metallic Substrates. *Nanoscale* **2021**, *13*, 14023–14034. [CrossRef]

31. Zhang, Y.; Zhou, S.; Lv, Z.; Fan, L.; Huang, Y.; Liu, X. A Facile Method to Prepare Superhydrophobic Coatings for Various Substrates. *Appl. Sci.* **2022**, *12*, 1240. [CrossRef]

32. Bai, H.; Tian, X.; Zheng, Y.; Ju, J.; Zhao, Y.; Jiang, L. Direction Controlled Driving of Tiny Water Drops on Bioinspired Artificial Spider Silks. *Adv. Mater.* **2010**, *22*, 5521–5525. [CrossRef]

33. Young, T. An Essay on the Cohesion of Fluids. *Philos. Trans. R. Soc.* **1805**, *95*, 65–87.

34. Wenzel, R.N. RESISTANCE OF SOLID SURFACES TO WETTING BY WATER. *Ind. Eng. Chem.* **1936**, *28*, 988–994. [CrossRef]

35. Cassie, A.B.D.; Baxter, S. Wettability of porous surfaces. *Trans. Faraday Soc.* **1944**, *40*, 546–551. [CrossRef]

36. Feng, L.; Zhang, Y.; Xi, J.; Zhu, Y.; Wang, N.; Xia, F.; Jiang, L. Petal Effect: A Superhydrophobic State with High Adhesive Force. *Langmuir* **2008**, *24*, 4114–4119. [CrossRef]

37. Wang, J.; Wang, C.; Wang, M.; Jiang, L. Effects of the distribution of micropapillae with nanofolds on the adhesive property of artificial red rose petals. *Chem. J. Chin. U* **2011**, *32*, 1807–1811.

38. Shao, Y.; Zhao, J.; Fan, Y.; Wan, Z.; Lu, L.; Zhang, Z.; Ming, W.; Ren, L. Shape memory superhydrophobic surface with switchable transition between "Lotus Effect" to "Rose Petal Effect". *Chem. Eng. J.* **2020**, *382*, 122989. [CrossRef]

39. Greenspan, H.P. On the motion of a small viscous droplet that wets a surface. *J. Fluid. Mech.* **1978**, *84*, 125–143. [CrossRef]

40. Chaudhury, M.K.; Whitesides, G.M. How to Make Water Run Uphill. *Science* **1992**, *256*, 1539–1541. [CrossRef] [PubMed]

41. Daniel, S.; Chaudhury, M.K.; Chen, J.C. Fast drop movements resulting from the phase change on a gradient surface. *Science* **2001**, *291*, 633–636. [CrossRef]

42. Feng, S.; Wang, S.; Gao, L.; Li, G.; Hou, Y.; Zheng, Y. Directional Water-Droplet Spreading on a High-Adhesion Surface. *Angew. Chem. Int. Ed.* **2014**, *53*, 6163–6167. [CrossRef]

43. Wang, R.; Hashimoto, K.; Fujishima, A.; Chikuni, M.; Kojima, E.; Kitamura, A.; Shimohigoshi, M.; Watanabe, T. Light-induced amphiphilic surfaces. *Nature* **1997**, *388*, 431–432. [CrossRef]

44. Ito, Y.; Heydari, M.; Hashimoto, A.; Konno, T.; Hirasawa, A.; Hori, S.; Kurita, K.; Nakajima, A. The Movement of a Water Droplet on a Gradient Surface Prepared by Photodegradation. *Langmuir* **2007**, *23*, 1845–1850. [CrossRef] [PubMed]

45. Hong, D.; Cho, W.K.; Kong, B.; Choi, I.S. Water-Collecting Capability of Radial-Wettability Gradient Surfaces Generated by Controlled Surface Reactions. *Langmuir* **2010**, *26*, 15080–15083. [CrossRef]

46. Hernández, S.C.; Bennett, C.J.C.; Junkermeier, C.E.; Tsoi, S.D.; Bezares, F.J.; Stine, R.; Robinson, J.T.; Lock, E.H.; Boris, D.R.; Pate, B.D.; et al. Chemical Gradients on Graphene To Drive Droplet Motion. *ACS Nano* **2013**, *7*, 4746–4755. [CrossRef]

47. He, B.; Lee, J. Dynamic wettability switching by surface roughness effect. In Proceedings of the The Sixteenth Annual International Conference On Micro Electro Mechanical Systems, Kyoto, Japan, 23 January 2003; Mems-03 Kyoto. IEEE: Kyoto, Japan, 2003; pp. 120–123.

48. Zhu, L.; Feng, Y.; Ye, X.; Zhou, Z. Tuning wettability and getting superhydrophobic surface by controlling surface roughness with well-designed microstructures. *Sens. Actuators A Phys.* **2006**, *130–131*, 595–600. [CrossRef]

49. Sun, C.; Zhao, X.; Han, Y.; Gu, Z.-Z. Control of water droplet motion by alteration of roughness gradient on silicon wafer by laser surface treatment. *Thin Solid Film.* **2008**, *516*, 4059–4063. [CrossRef]

50. Chu, K.; Xiao, R.; Wang, E.N. Uni-directional liquid spreading on asymmetric nanostructured surfaces. *Nat. Mater.* **2010**, *9*, 413–417. [CrossRef]

51. Li, Y.; Zhang, Q.; Wei, X.; Li, K.; Tian, D.; Jiang, L. Curvature Adjustable Liquid Transport on Anisotropic Microstructured Elastic Film. *ACS Nano* **2023**, *17*, 6036–6044. [CrossRef]

52. Bliznyuk, O.; Jansen, H.P.; Kooij, E.S.; Zandvliet, H.J.W.; Poelsema, B. Smart Design of Stripe-Patterned Gradient Surfaces to Control Droplet Motion. *Langmuir* **2011**, *27*, 11238–11245. [CrossRef]

53. Liu, C.; Sun, J.; Li, J.; Xiang, C.; Che, L.; Wang, Z.; Zhou, X. Long-range spontaneous droplet self-propulsion on wettability gradient surfaces. *Sci. Rep.* **2017**, *7*, 7552. [CrossRef]

54. Huang, D.; Leu, T. Fabrication of high wettability gradient on copper substrate. *Appl. Surf. Sci.* **2013**, *280*, 25–32. [CrossRef]

55. Liao, Q.; Wang, H.; Zhu, X.; Gu, B. Experimental Study for Movement of Liquid Drop on the Surface with Gradient Surface Energy. In Proceedings of the 9th AIAA/ASME Joint Thermophysics and Heat Transfer Conference, San Francisco, CA, USA, 5–8 June 2006; American Institute of Aeronautics and Astronautics: Reston, VA, USA, 2006.

56. Hauksbee, F. An Account of an Experiment Touching the Ascent of Water between Two Glass Planes, in an Hyperbolick Figure. By Mr. Francis Hauksbee, F.R.S. *Philos. Trans. (1683–1775)* **1710**, *27*, 539–540.

57. Prakash, M.; Quéré, D.; Bush, J.W.M. Surface Tension Transport of Prey by Feeding Shorebirds: The Capillary Ratchet. *Science* **2008**, *320*, 931–934. [CrossRef]

58. Bush, J.W.M.; Peaudecerf, F.; Prakash, M.; Quéré, D. On a tweezer for droplets. *Adv. Colloid. Interface* **2010**, *161*, 10–14. [CrossRef]

59. Carroll, B.J. Equilibrium conformations of liquid drops on thin cylinders under forces of capillarity. A theory for the roll-up process. *Langmuir* **1986**, *2*, 248–250. [CrossRef]

60. Mchale, G.; Newton, M.I.; Carroll, B.J. The Shape and Stability of Small Liquid Drops on Fibers. *Oil Gas Sci. Technol.* **2001**, *56*, 47–54. [CrossRef]

61. McHale, G.; Newton, M.I. Global geometry and the equilibrium shapes of liquid drops on fibers. *Colloids Surf. A Physicochem. Eng. Asp.* **2002**, *206*, 79–86. [CrossRef]

62. LORENCEAU, E.; QUERE, D. Drops on a conical wire. *J. Fluid. Mech.* **2004**, *510*, 29–45. [CrossRef]

63. Xue, Y.; Wang, T.; Shi, W.; Sun, L.; Zheng, Y. Water collection abilities of green bristlegrass bristle. *RSC Adv.* **2014**, *4*, 40837–40840. [CrossRef]

64. Chen, D.; Niu, S.; Zhang, J.; Mu, Z.; Chen, H.; Zhang, D.; Yao, Z.; Han, Z.; Ren, L. Superfast Liquid Transfer Strategy Through Sliding on a Liquid Membrane Inspired from Scorpion Setae. *Adv. Mater. Interfaces* **2018**, *5*, 1800802. [CrossRef]

65. Zheng, Y.; Bai, H.; Huang, Z.; Tian, X.; Nie, F.-Q.; Zhao, Y.; Zhai, J.; Jiang, L. Directional water collection on wetted spider silk. *Nature* **2010**, *463*, 640–643. [CrossRef]

66. Park, K.; Kim, P.; Grinthal, A.; He, N.; Fox, D.; Weaver, J.C.; Aizenberg, J. Condensation on slippery asymmetric bumps. *Nature* **2016**, *531*, 78–82. [CrossRef] [PubMed]

67. Feng, S.; Wang, Q.; Xing, Y.; Hou, Y.; Zheng, Y. Continuous Directional Water Transport on Integrating Tapered Surfaces. *Adv. Mater. Interfaces* **2020**, *7*, 2000081. [CrossRef]

68. Seo, J.; Lee, S.; Lee, J.; Lee, T. Guided transport of water droplets on superhydrophobic-hydrophilic patterned Si nanowires. *ACS Appl. Mater. Interfaces* **2011**, *3*, 4722–4729. [CrossRef]

69. Schutzius, T.M.; Elsharkawy, M.; Tiwari, M.K.; Megaridis, C.M. Surface tension confined (STC) tracks for capillary-driven transport of low surface tension liquids. *Lab Chip* **2012**, *12*, 5237–5242. [CrossRef] [PubMed]

70. Xing, S.; Harake, R.S.; Pan, T. Droplet-driven transports on superhydrophobic-patterned surface microfluidics. *Lab Chip* **2011**, *11*, 3642–3648. [CrossRef]

71. Alheshibri, M.H.; Rogers, N.G.; Sommers, A.D.; Eid, K.F. Spontaneous movement of water droplets on patterned Cu and Al surfaces with wedge-shaped gradients. *Appl. Phys. Lett.* **2013**, *102*, 174103. [CrossRef]

72. Ghosh, A.; Ganguly, R.; Schutzius, T.M.; Megaridis, C.M. Wettability patterning for high-rate, pumpless fluid transport on open, non-planar microfluidic platforms. *Lab Chip* **2014**, *14*, 1538–1550. [CrossRef]

73. Liu, J.; Yan, D.; Zhou, Y.; Chen, Y.; Liu, X.; Zhao, D.; Liu, J.; Sun, J. Droplet motion on superhydrophobic/superhydrophilic wedge-shaped patterned surfaces with different micro-morphologies. *Colloids Surf. A Physicochem. Eng. Asp.* **2022**, *647*, 128999. [CrossRef]

74. Liu, Z.; Liu, H.; Li, W.; Song, J. Optimization of bioinspired surfaces with enhanced water transportation capacity. *Chem. Eng. J.* **2022**, *433*, 134568. [CrossRef]

75. Xie, D.; Zhang, B.Y.; Wang, G.; Sun, Y.; Wu, C.; Ding, G. High-Performance Directional Water Transport Using a Two-Dimensional Periodic Janus Gradient Structure. *Small Methods* **2022**, *6*, 2200812. [CrossRef]

76. Liu, Q.; Zhang, J.; Sun, P.; Wang, J.; Zhao, W.; Zhao, G.; Chen, N.; Yang, Y.; Li, L.; He, N.; et al. Achieving ultralong directional liquid transportation spontaneously with a high velocity. *J. Mater. Chem. A* **2023**, *11*, 10164–10173. [CrossRef]

77. Yan, D.; Lu, Y.; Liu, J.; Chen, Y.; Sun, J.; Song, J. Enhanced water transportation on a superhydrophilic serial cycloid-shaped pattern. *Nanoscale* **2023**, *15*, 11473–11481. [CrossRef] [PubMed]

78. Shah, I.; Kim, S.W.; Kim, K.; Doh, Y.H.; Choi, K.H. Experimental and numerical analysis of Y-shaped split and recombination micro-mixer with different mixing units. *Chem. Eng. J.* **2019**, *358*, 691–706. [CrossRef]

79. Irfan, M.; Shah, I.; Niazi, U.M.; Ali, M.; Ali, S.; Jalalah, M.S.; Khan, M.K.A.; Almawgani, A.H.M.; Rahman, S. Numerical analysis of non-aligned inputs M-type micromixers with different shaped obstacles for biomedical applications. *Proc. Inst. Mech. Eng. Part E J. Process Mech. Eng.* **2021**, *236*, 870–880. [CrossRef]

80. Sherbrooke, W.C. Rain-Harvesting in the Lizard, Phrynosoma cornutum: Behavior and Integumental Morphology. *J. Herpetol.* **1990**, *24*, 302–308. [CrossRef]

81. Comanns, P.; Effertz, C.; Hischen, F.; Staudt, K.; Böhme, W.; Baumgartner, W. Moisture harvesting and water transport through specialized micro-structures on the integument of lizards. *Beilstein J. Nanotechnol.* **2011**, *2*, 204–214. [CrossRef]

82. Comanns, P.; Buchberger, G.; Buchsbaum, A.; Baumgartner, R.; Kogler, A.; Bauer, S.; Baumgartner, W. Directional, passive liquid transport: The Texas horned lizard as a model for a biomimetic 'liquid diode'. *J. R. Soc. Interface* **2015**, *12*, 20150415. [CrossRef]

83. Comanns, P.; Winands, K.; Arntz, K.; Klocke, F.; Baumgartner, W. Laser-Based biomimetic functionalization of surfaces: From moisture harvesting lizards to specific fluid transport systems. *Int. J. Des. Nat. Ecodyn.* **2014**, *9*, 206–215. [CrossRef]

84. Buchberger, G.; Hischen, F.; Comanns, P.; Baumgartner, R.; Kogler, A.; Buchsbaum, A.; Bauer, S.; Baumgartner, W. Bio-inspired Microfluidic Devices for Passive, Directional Liquid Transport: Model-based Adaption for Different Materials. *Procedia Eng.* **2015**, *120*, 106–111. [CrossRef]

85. Bohn, H.F.; Federle, W. Insect aquaplaning: Nepenthes pitcher plants capture prey with the peristome, a fully wettable water-lubricated anisotropic surface. *Proc Natl. Acad. Sci. USA* **2004**, *101*, 14138–14143. [CrossRef] [PubMed]

86. Chen, H.; Zhang, L.; Zhang, P.; Zhang, D.; Han, Z.; Jiang, L. A Novel Bioinspired Continuous Unidirectional Liquid Spreading Surface Structure from the Peristome Surface of *Nepenthes alata*. *Small* **2017**, *13*, 1601676. [CrossRef]

87. Zhang, P.; Zhang, L.; Chen, H.; Dong, Z.; Zhang, D. Surfaces Inspired by the Nepenthes Peristome for Unidirectional Liquid Transport. *Adv. Mater.* **2017**, *29*, 1702995. [CrossRef]

88. Li, C.; Li, N.; Zhang, X.; Dong, Z.; Chen, H.; Jiang, L. Uni-Directional Transportation on Peristome-Mimetic Surfaces for Completely Wetting Liquids. *Angew. Chem. Int. Ed.* **2016**, *55*, 14988–14992. [CrossRef] [PubMed]

89. Li, J.; Zhou, X.; Li, J.; Che, L.; Yao, J.; McHale, G.; Chaudhury, M.K.; Wang, Z. Topological liquid diode. *Sci. Adv.* **2017**, *3*, eaao3530. [CrossRef] [PubMed]

90. Li, J.; Zheng, H.; Zhou, X.; Zhang, C.; Liu, M.; Wang, Z. Flexible topological liquid diode catheter. *Mater. Today Phys.* **2020**, *12*, 100170. [CrossRef]

91. Geng, H.; Bai, H.; Fan, Y.; Wang, S.; Ba, T.; Yu, C.; Cao, M.; Jiang, L. Unidirectional water delivery on a superhydrophilic surface with two-dimensional asymmetrical wettability barriers. *Mater. Horiz.* **2018**, *5*, 303–308. [CrossRef]

92. Feng, S.; Zhu, P.; Zheng, H.; Zhan, H.; Chen, C.; Li, J.; Wang, L.; Yao, X.; Liu, Y.; Wang, Z. Three-dimensional capillary ratchet-induced liquid directional steering. *Science* **2021**, *373*, 1344–1348. [CrossRef]

93. Feng, S.; Delannoy, J.; Malod, A.; Zheng, H.; Quéré, D.; Wang, Z. Tip-induced flipping of droplets on Janus pillars: From local reconfiguration to global transport. *Sci. Adv.* **2020**, *6*, eabb4540. [CrossRef] [PubMed]

94. Wu, H.; Mendel, N.; van der Ham, S.; Shui, L.; Zhou, G.; Mugele, F. Charge Trapping-Based Electricity Generator (CTEG): An Ultrarobust and High Efficiency Nanogenerator for Energy Harvesting from Water Droplets. *Adv. Mater.* **2020**, *32*, 2001699. [CrossRef] [PubMed]

95. Chen, W.; Xiang, Y.; Kong, X.; Wen, L. Polymer-based membranes for promoting osmotic energy conversion. *Giant* **2022**, *10*, 100094. [CrossRef]

96. Mai, V.; Lee, T.; Yang, R. Enhanced-performance droplet-triboelectric nanogenerators with composite polymer films and electrowetting-assisted charge injection. *Energy* **2022**, *260*, 125173. [CrossRef]

97. Chen, Y.; He, J.; Wang, L.; Xue, Y.; Zheng, Y.; Jiang, L. Excellent bead-on-string silkworm silk with drop capturing abilities. *J. Mater. Chem.* **2014**, *2*, 1230–1234. [CrossRef]

98. Deng, S.; Shang, W.; Feng, S.; Zhu, S.; Xing, Y.; Li, D.; Hou, Y.; Zheng, Y. Controlled droplet transport to target on a high adhesion surface with multi-gradients. *Sci. Rep.* **2017**, *7*, 45687. [CrossRef] [PubMed]

99. Chen, H.; Ran, T.; Gan, Y.; Zhou, J.; Zhang, Y.; Zhang, L.; Zhang, D.; Jiang, L. Ultrafast water harvesting and transport in hierarchical microchannels. *Nat. Mater.* **2018**, *17*, 935–942. [CrossRef]

100. Xu, C.; Feng, R.; Song, F.; Wang, X.-L.; Wang, Y.-Z. Desert Beetle-Inspired Superhydrophilic/Superhydrophobic Patterned Cellulose Film with Efficient Water Collection and Antibacterial Performance. *ACS Sustain. Chem. Eng.* **2018**, *6*, 14679–14684. [CrossRef]

101. Ju, J.; Xiao, K.; Yao, X.; Bai, H.; Jiang, L. Bioinspired Conical Copper Wire with Gradient Wettability for Continuous and Efficient Fog Collection. *Adv. Mater.* **2013**, *25*, 5937–5942. [CrossRef]

102. Bai, H.; Wang, L.; Ju, J.; Sun, R.; Zheng, Y.; Jiang, L. Efficient Water Collection on Integrative Bioinspired Surfaces with Star-Shaped Wettability Patterns. *Adv. Mater.* **2014**, *26*, 5025–5030. [CrossRef]

103. Wu, W.; Haoyu, B.; Yang, Y.; Li, G.; Chen, Z.; Tang, C.; Yin, H.; Lai, L.; Liu, J.; Xuan, S.; et al. Sequence liquid manipulation on a multifunctional snowflake-patterned interface with dual unidirectional wettability. *J. Mater. Chem. A* **2023**, *11*, 873–8885. [CrossRef]

104. Yan, D.; Chen, Y.; Liu, J.; Song, J. Super-Fast Fog Collector Based on Self-Driven Jet of Mini Fog Droplets. *Small* **2023**, 2301745. [CrossRef] [PubMed]

105. Feng, L.; Zhang, Z.; Mai, Z.; Ma, Y.; Liu, B.; Jiang, L.; Zhu, D. A Super-Hydrophobic and Super-Oleophilic Coating Mesh Film for the Separation of Oil and Water. *Angew. Chem. Int. Ed.* **2004**, *43*, 2012–2014. [CrossRef] [PubMed]

106. Li, C.; Wu, L.; Yu, C.; Dong, Z.; Jiang, L. Peristome-Mimetic Curved Surface for Spontaneous and Directional Separation of Micro Water-in-Oil Drops. *Angew. Chem. Int. Ed.* **2017**, *56*, 13623–13628. [CrossRef] [PubMed]

107. Yang, X.; Song, J.; Zheng, H.; Deng, X.; Liu, X.; Lu, X.; Sun, J.; Zhao, D. Anisotropic sliding on dual-rail hydrophilic tracks. *Lab Chip* **2017**, *17*, 1041–1050. [CrossRef] [PubMed]

108. Koukoravas, T.P.; Ghosh, A.; Mahapatra, P.S.; Ganguly, R.; Megaridis, C.M. Spatially-selective cooling by liquid jet impinging orthogonally on a wettability-patterned surface. *Int. J. Heat. Mass. Transf.* **2016**, *95*, 142–152. [CrossRef]

109. Koukoravas, T.P.; Sinha Mahapatra, P.; Ganguly, R.; Megaridis, C.M. Wettability-confined liquid-film convective cooling: Parameter study. *Int. J. Heat. Mass. Transf.* **2018**, *126*, 667–676. [CrossRef]

110. Yan, S.; Ren, F.; Li, C.; Jiao, Y.; Wang, C.; Wu, S.; Wei, S.; Hu, Y.; Li, J.; Xiao, Y.; et al. Unidirectional self-transport of air bubble via a Janus membrane in aqueous environment. *Appl. Phys. Lett.* **2018**, *113*, 261602. [CrossRef]

111. Huo, J.; Yang, Q.; Yong, J.; Fan, P.; Lu, Y.F.; Hou, X.; Chen, F. Underwater Superaerophobicity/Superaerophilicity and Unidirectional Bubble Passage Based on the Femtosecond Laser-Structured Stainless Steel Mesh. *Adv. Mater. Interfaces* **2020**, *7*, 1902128. [CrossRef]

112. Dai, X.; Guo, Z.; Liu, W. Ultraviolet-Driven Janus Foams with Wetting Gradients: Unidirectional Penetration Control for Underwater Bubbles. *ACS Appl. Mater. Interfaces* **2022**, *14*, 42734–42743. [CrossRef]

113. Yong, J.; Chen, F.; Huo, J.; Fang, Y.; Yang, Q.; Zhang, J.; Hou, X. Femtosecond laser induced underwater superaerophilic and superaerophobic PDMS sheets with through microholes for selective passage of air bubbles and further collection of underwater gas. *Nanoscale* **2018**, *10*, 3688–3696. [CrossRef]

114. Yong, J.; Chen, F.; Fang, Y.; Huo, J.; Yang, Q.; Zhang, J.; Bian, H.; Hou, X. Bioinspired Design of Underwater Superaerophobic and Superaerophilic Surfaces by Femtosecond Laser Ablation for Anti- or Capturing Bubbles. *ACS Appl. Mater. Interfaces* **2017**, *9*, 39863–39871. [CrossRef]

115. Tahzibi, H.; Azizian, S.; Szunerits, S.; Boukherroub, R. Fast Capture, Collection, and Targeted Transfer of Underwater Gas Bubbles Using Janus-Faced Carbon Cloth Prepared by a Novel and Simple Strategy. *ACS Appl. Mater. Interfaces* **2022**, *14*, 45013–45024. [CrossRef]

116. Yin, K.; Yang, S.; Dong, X.; Chu, D.; Duan, J.-A.; He, J. Robust laser-structured asymmetrical PTFE mesh for underwater directional transportation and continuous collection of gas bubbles. *Appl. Phys. Lett.* **2018**, *112*, 243701. [CrossRef]

117. Yong, J.; Yang, Q.; Huo, J.; Hou, X.; Chen, F. Underwater gas self-transportation along femtosecond laser-written open superhydrophobic surface microchannels (<100 μm) for bubble/gas manipulation. *Int. J. Extrem. Manuf.* **2022**, *4*, 15002. [CrossRef]

118. Xie, D.; Sun, Y.; Wu, Y.; Wang, K.; Wang, G.; Zang, F.; Ding, G. Engineered Switchable-Wettability Surfaces for Multi-Path Directional Transportation of Droplets and Subaqueous Bubbles. *Adv. Mater.* **2023**, *35*, 2208645. [CrossRef]

119. Yu, C.; Cao, M.; Dong, Z.; Wang, J.; Li, K.; Jiang, L. Spontaneous and Directional Transportation of Gas Bubbles on Superhydrophobic Cones. *Adv. Funct. Mater.* **2016**, *26*, 3236–3243. [CrossRef]

120. Xiao, X.; Zhang, C.; Ma, H.; Zhang, Y.; Liu, G.; Cao, M.; Yu, C.; Jiang, L. Bioinspired Slippery Cone for Controllable Manipulation of Gas Bubbles in Low-Surface-Tension Environment. *ACS Nano* **2019**, *13*, 4083–4090. [CrossRef]

121. Xue, X.; Yu, C.; Wang, J.; Jiang, L. Superhydrophobic Cones for Continuous Collection and Directional Transportation of CO_2 Microbubbles in CO_2 Supersaturated Solutions. *ACS Nano* **2016**, *10*, 10887–10893. [CrossRef]

122. Yu, C.; Zhu, X.; Cao, M.; Yu, C.; Li, K.; Jiang, L. Superhydrophobic helix: Controllable and directional bubble transport in an aqueous environment. *J. Mater. Chem. A* **2016**, *4*, 16865–16870. [CrossRef]

123. Shi, D.; Chen, Y.; Yao, Y.; Hou, M.; Chen, X.; Gao, J.; He, Y.; Zhang, G.; Wong, C.-P. Ladderlike Conical Micropillars Facilitating Underwater Gas-Bubble Manipulation in an Aqueous Environment. *ACS Appl. Mater. Interfaces* **2020**, *12*, 42437–42445. [CrossRef] [PubMed]

124. Ma, H.; Cao, M.; Zhang, C.; Bei, Z.; Li, K.; Yu, C.; Jiang, L. Directional and Continuous Transport of Gas Bubbles on Superaerophilic Geometry-Gradient Surfaces in Aqueous Environments. *Adv. Funct. Mater.* **2018**, *28*, 1705091. [CrossRef]

125. Liu, Z.; Zhang, H.; Han, Y.; Huang, L.; Chen, Y.; Liu, J.; Wang, X.; Liu, X.; Ling, S. Superaerophilic Wedge-Shaped Channels with Precovered Air Film for Efficient Subaqueous Bubbles/Jet Transportation and Continuous Oxygen Supplementation. *ACS Appl. Mater. Interfaces* **2019**, *11*, 23808–23814. [CrossRef] [PubMed]

126. Song, J.; Liu, Z.; Wang, X.; Liu, H.; Lu, Y.; Deng, X.; Carmalt, C.J.; Parkin, I.P. High-efficiency bubble transportation in an aqueous environment on a serial wedge-shaped wettability pattern. *J. Mater. Chem. A* **2019**, *7*, 13567–13576. [CrossRef]

127. Long, Z.; Zhao, Y.; Zhang, C.; Zhang, Y.; Yu, C.; Wu, Y.; Ma, J.; Cao, M.; Jiang, L. A Multi-Bioinspired Dual-Gradient Electrode for Microbubble Manipulation toward Controllable Water Splitting. *Adv. Mater.* **2020**, *32*, 1908099. [CrossRef]

128. Xiao, X.; Li, S.; Zhu, X.; Zhang, C.; Jiang, F.; Yu, C.; Jiang, L. Bioinspired Two-Dimensional Structure with Asymmetric Wettability Barriers for Unidirectional and Long-Distance Gas Bubble Delivery Underwater. *Nano Lett.* **2021**, *21*, 2117–2123. [CrossRef]

129. Ning, Y.; Zhang, D.; Ben, S.; Zhao, Z.; Zha, J.; Tian, D.; Liu, K.; Jiang, L. An Innovative Design by Single-Layer Superaerophobic Mesh: Continuous Underwater Bubble Antibuoyancy Collection and Transportation. *Adv. Funct. Mater.* **2020**, *30*, 1907027. [CrossRef]

130. Yu, C.; Cao, M.; Dong, Z.; Li, K.; Yu, C.; Wang, J.; Jiang, L. Aerophilic Electrode with Cone Shape for Continuous Generation and Efficient Collection of H_2 Bubbles. *Adv. Funct. Mater.* **2016**, *26*, 6830–6835. [CrossRef]

131. Xue, X.; Wang, R.; Lan, L.; Wang, J.; Xue, Z.; Jiang, L. Reliable Manipulation of Gas Bubble Size on Superaerophilic Cones in Aqueous Media. *ACS Appl. Mater. Interfaces* **2018**, *10*, 5099–5106. [CrossRef]

132. Han, K.; Yong, K. Overcoming Limitations in Surface Geometry-Driven Bubble Transport: Bidirectional and Unrestricted Movement of an Underwater Gas Bubble Using a Magnetocontrollable Nonwetting Surface. *Adv. Funct. Mater.* **2021**, *31*, 2101970. [CrossRef]